Technical Report: Degenerate Motions of Multisensor Fusion-based Navigation

Woosik Lee - woosik@udel.edu
Chuchu Chen - ccchu@udel.edu
Guoquan Huang - ghuang@udel.edu

Department of Mechanical Engineering
University of Delaware, Delaware, USA

RPNG

Robot Perception and Navigation Group (RPNG)
Technical Report: Degenerate Motions of Multisensor Fusion-based Navigation
Last Updated - September 28, 2023

Contents

Table 1: Summary of degenerate motions.

Degenerate Motions	Partially Unobservable States	Lemmas
1 Axis Rotation & 3 Axis Translation	${}^{G}\mathbf{p}_I,\ {}^{J}\mathbf{p}_I$	*Lemma 2.2, 3.2*
⌞ Constant Linear & Angular Velocities	${}^{G}\mathbf{p}_I,\ {}^{J}_{I}\bar{q},\ {}^{J}\mathbf{p}_I,\ {}^{J}t_I$	*Lemma 2.3, 3.3*
⌞ 3 Axis Translation	${}^{G}\mathbf{p}_I,\ {}^{J}\mathbf{p}_I$	*Lemma 2.4, 3.4*
⌞ 2 Axis Translation	${}^{G}\mathbf{p}_I,\ {}^{J}\mathbf{p}_I$	*Lemma 2.4, 3.4*
⌞ 1 Axis Translation	${}^{I}_{G}\bar{q},\ {}^{G}\mathbf{p}_I,\ {}^{J}_{I}\bar{q},\ {}^{J}\mathbf{p}_I$	*Lemma 2.5, 3.5*
⌞ Constant Linear Velocity	${}^{I}_{G}\bar{q},\ {}^{G}\mathbf{p}_I,\ {}^{J}_{I}\bar{q},\ {}^{J}\mathbf{p}_I,\ {}^{J}t_I$	*Lemma 2.6, 3.6*
⌞ 1 Axis Rotation	${}^{I}_{G}\bar{q},\ {}^{G}\mathbf{p}_I,\ {}^{J}_{I}\bar{q},\ {}^{J}\mathbf{p}_I$	*Lemma 2.7, 3.7*
⌞ Constant Angular Velocity	${}^{I}_{G}\bar{q},\ {}^{G}\mathbf{p}_I,\ {}^{J}_{I}\bar{q},\ {}^{J}\mathbf{p}_I,\ {}^{J}t_I$	*Lemma 2.8, 3.8*
⌞ No Motion	${}^{I}_{G}\bar{q},\ {}^{G}\mathbf{p}_I,\ {}^{J}_{I}\bar{q},\ {}^{J}\mathbf{p}_I,\ {}^{J}t_I$	*Lemma 2.9, 3.9*

1 Introduction

In this work, we provide degenerate motion analysis on general local and global sensor-paired systems identifying 9 degenerate motions (see Tab. 1 for the summary) which can be applied to many existing navigation systems. Comprehensive numerical studies are conducted to verify those identified motions, show the effect of degenerate motion on state estimation, and demonstrate the generalizability of our analysis on various multi-sensor systems. Specifically, we show the following:

- Analyzed both synchronous and asynchronous multi-sensor systems equipped with local and global sensors performing spatiotemporal calibration and identified 9 degenerate motions that make the systems' state partially unobservable.
- Verified degenerate motions with both observability analysis and numerical study which shows the state estimation error accumulates over time towards exactly the unobservable directions induced by each degenerate motion.
- Conducted numerical study with different levels of local sensor measurement noises showing the relevance to the amount of state estimation drift under degenerate motions.
- Showed the generalizability of our analysis by verifying different combinations of multi-sensor systems, e.g., IMU-GPS, IMU-camera, IMU-LiDAR, and IMU-GPS-camera-LiDAR, have the same estimation drift under the identified motions.

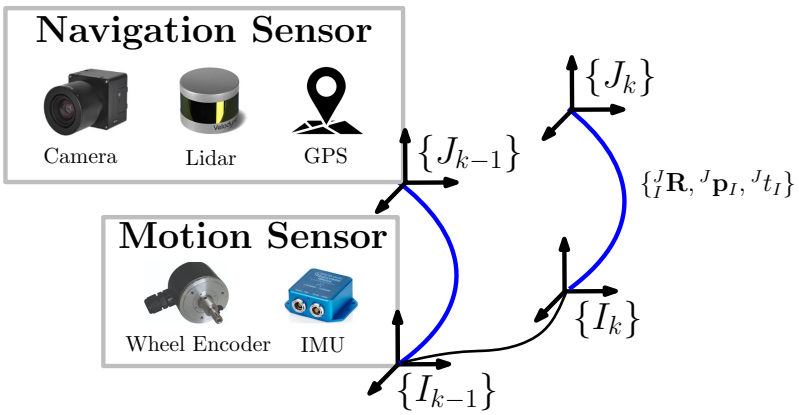

Figure 1: Exemplary combinations of the multi-sensor system with local motion sensor $\{I\}$ and global navigation sensor $\{J\}$ navigates from time t_{k-1} to t_k. While camera or LiDAR sensors are typically not considered global sensors, they can provide global information with map or place recognition.

1.1 Setups Used for Numerical Study

In the following sections, we provide mathematical proofs of identified degenerate motions and present our numerical study results along with them conducted in our simulation leveraging MINS [1]. Specifically, we simulate realistic inertial angular velocity and linear acceleration measurements (IMU) as the local motion sensor to perform state propagation. We also simulate a global navigation sensor that measures the 6 DoF pose of the sensor (tagged VICON). In the later sections, we extended our study to multi-sensor systems, additionally simulating camera, GPS, and LiDAR measurements and fusing them within MINS estimator. The simulation parameters used in the numerical study are summarized in Tab. 2.

Table 2: Simulation parameters and prior single standard deviations that perturbations of measurements and initial states were drawn from.

IMU		**VICON**		**Camera**		**GPS**		**LiDAR**	
Freq. (Hz)	200	Freq. (Hz)	20	Freq. (Hz)	30	Freq. (Hz)	25	Freq. (Hz)	10
Accel. Noise	1e-2	Ori. Noise (rad)	1e-1	Noise (px)	1	Noise (m)	1e-1	# of points	3k
Accel. Rand. Walk	5e-6	Pos. Noise (m)	1e-1	Ext (Ori). Ptrb.	1e-4	Ext (Pos). Ptrb.	1e-3	Noise (m)	1e-1
Gyro. Noise	1e-2	Ext (Ori). Ptrb.	1e-4	Ext (Pos). Ptrb.	1e-3	Toff. Ptrb.	1e-3	Ext (Ori). Ptrb.	1e-4
Gyro. Rand. Walk	5e-6	Ext (Pos). Ptrb.	1e-3	Toff. Ptrb.	1e-4			Ext (Pos). Ptrb.	1e-3
		Toff. Ptrb.	1e-4					Toff. Ptrb.	1e-4
		Ext (Pos). ${}^{J}\mathbf{p}_{I}$	$\begin{bmatrix}1\\1\\1\end{bmatrix}$	Ext (Pos). ${}^{C}\mathbf{p}_{I}$	$\begin{bmatrix}-0.01\\0.01\\0.01\end{bmatrix}$	Ext (Pos). ${}^{I}\mathbf{p}_{G}$	$\begin{bmatrix}1\\1\\1\end{bmatrix}$	Ext (Pos). ${}^{L}\mathbf{p}_{I}$	$\begin{bmatrix}0.1\\0.1\\0.1\end{bmatrix}$
		Ext (Ori). (r,p,y)	$\begin{bmatrix}0\\0\\0\end{bmatrix}$	Ext (Ori). (r,p,y)	$\begin{bmatrix}90\\0\\0\end{bmatrix}$			Ext (Ori). (r,p,y)	$\begin{bmatrix}15\\0\\0\end{bmatrix}$

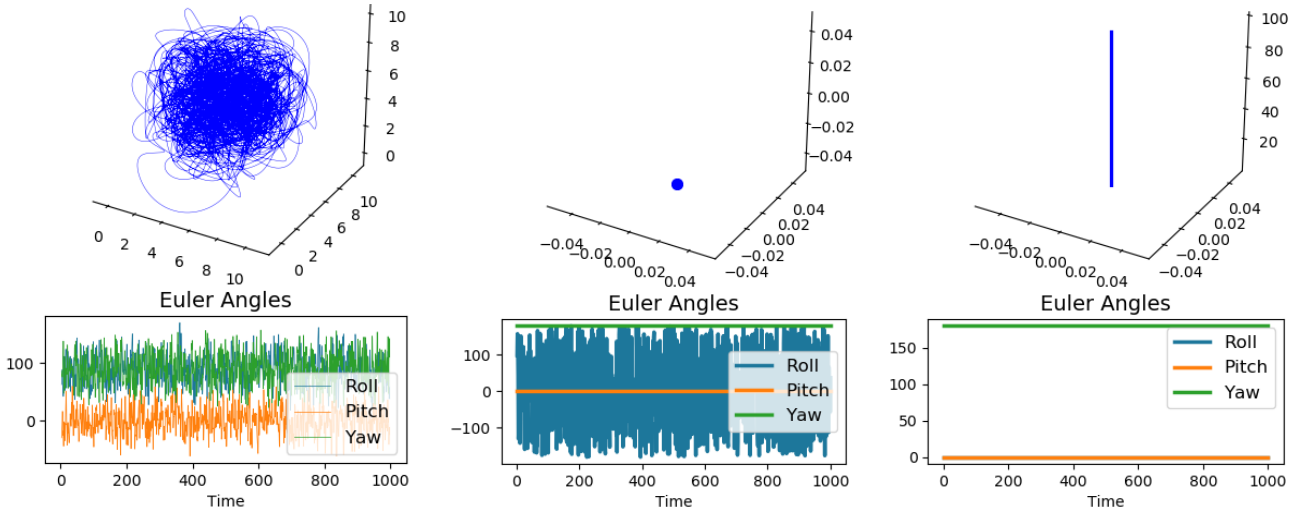

(a) General 3D motion trajectory (b) 1-axis rotation trajectory (c) 1-axis translation trajectory

Figure 2: Examplary trajectories used for the numerical study.

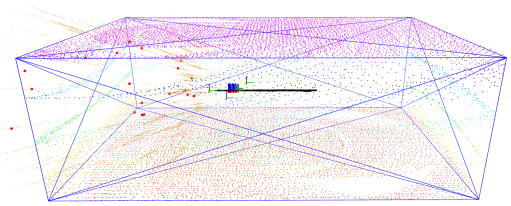

Figure 3: Examplary simulation environment for numerical study of LiDAR and cameras. The blue box indicates simulated walls the LiDAR points to hit, red and orange dots are camera point features.

2 Degenerate Motions: Synchronous Global and Local Sensor Pair

In this section, we analyze degenerate motion using synchronized measurements from two general sensors: $\{I\}$, providing ego-motion information (e.g., IMU or wheel), and $\{J\}$, receiving global pose measurements (e.g., GPS or motion tracking). We assume noise-free for the analysis.

2.1 State to Analyze

At time t_k, the state vector carries the current pose of sensor $\{I\}$ and the spatiotemporal calibration parameters:

$$\mathbf{x}_{\mathbf{S}_k} = \begin{bmatrix} {}^{I_k}_{G}\bar{q}^\top & {}^{G}\mathbf{p}_{I_k}^\top & {}^{J}_{I}\bar{q}^\top & {}^{J}\mathbf{p}_{I}^\top & {}^{J}t_I \end{bmatrix}^\top \tag{1}$$

where ${}^{I_k}_{G}\bar{q}$ is the unit quaternion (${}^{I_k}_{G}\mathbf{R}$ in rotation matrix form) that represents the rotation from the global $\{G\}$ to the sensor $\{I\}$; ${}^{G}\mathbf{p}_{I_k}$ is the sensor $\{I\}$ position in the global $\{G\}$; $\{{}^{J}_{I}\bar{q}, {}^{J}\mathbf{p}_I\}$ and ${}^{J}t_I$ are the extrinsic calibration and time offset between sensor $\{I\}$ and $\{J\}$. Additionally, the corresponding error state vector is:

$$\tilde{\mathbf{x}}_{\mathbf{S}_k} = \begin{bmatrix} {}^{I_k}_{G}\tilde{\boldsymbol{\theta}}^\top & {}^{G}\tilde{\mathbf{p}}_{I_k}^\top & {}^{J}_{I}\tilde{\boldsymbol{\theta}}^\top & {}^{J}\tilde{\mathbf{p}}_{I}^\top & {}^{J}\tilde{t}_I \end{bmatrix}^\top \tag{2}$$

Note that throughout the paper, $\hat{\mathbf{x}}$ is used to denote the estimate of a random variable $\mathbf{x}$ with $\tilde{\mathbf{x}} = \mathbf{x} \boxminus \hat{\mathbf{x}}$ denotes the error state. For the quaternion error state, we employ JPL multiplicative error [2] and use $\tilde{\boldsymbol{\theta}} \in \mathbb{R}^3$ defined by the error quaternion i.e., $\tilde{\bar{q}} = \bar{q} \otimes \hat{\bar{q}}^{-1} \simeq [\frac{1}{2}\tilde{\boldsymbol{\theta}}^\top \; 1]^\top$. The $\boxplus$ and $\boxminus$ operations map elements to and from a given manifold and equate to simple + and - for vector variables [3].

2.2 State Propagation model with Local Sensor $\{I\}$

At time t_k, we leverage the local sensor's relative pose information, $\{{}^{I_k}_{I_{k-1}}\bar{q}, {}^{I_{k-1}}\mathbf{p}_{I_k}\}$, to propagate the state, Eq. (1), from t_{k-1} to t_k as:

$${}^{I_k}_{G}\bar{q} = {}^{I_k}_{I_{k-1}}\bar{q} \boxplus {}^{I_{k-1}}_{G}\bar{q}, \;\; {}^{G}\mathbf{p}_{I_k} = {}^{G}\mathbf{p}_{I_{k-1}} + {}^{G}_{I_{k-1}}\mathbf{R}\,{}^{I_{k-1}}\mathbf{p}_{I_k} \tag{3}$$

while the calibration states remain the same. The corresponding error state transition can be shown as:

$$\tilde{\mathbf{x}}_{\mathbf{S}_k} = \boldsymbol{\Phi}_{\mathbf{S}}(t_k, t_{k-1})\tilde{\mathbf{x}}_{\mathbf{S}_{k-1}} \tag{4}$$

$$\boldsymbol{\Phi}_{\mathbf{S}}(t_k, t_{k-1}) = \begin{bmatrix} {}^{I_k}_{I_{k-1}}\mathbf{R} & \mathbf{0}_3 & \mathbf{0}_{3\times 7} \\ -{}^{G}_{I_{k-1}}\mathbf{R}\lfloor {}^{I_{k-1}}\mathbf{p}_{I_k} \rfloor & \mathbf{I}_3 & \mathbf{0}_{3\times 7} \\ \mathbf{0}_{7\times 3} & \mathbf{0}_{7\times 3} & \mathbf{I}_7 \end{bmatrix} \tag{5}$$

where $\lfloor \cdot \rfloor$ is a skew-symmetric matrix.

2.3 State Update model with Global Sensor $\{J\}$

The synchronized global sensor, $\{J\}$, measures the 6 DOF pose of the sensor in global at the exact state time t_k as:

$$\mathbf{z}_{\mathbf{S}_k} := \begin{bmatrix} {}^{J_k}_{G}\boldsymbol{\theta} \\ {}^{G}\mathbf{p}_{J_k} \end{bmatrix} = \begin{bmatrix} \mathrm{Log}({}^{J}_{I}\mathbf{R}\,{}^{I_k}_{G}\mathbf{R}) \\ {}^{G}\mathbf{p}_{I_k} + {}^{G}_{I_k}\mathbf{R}\,{}^{I}\mathbf{p}_J \end{bmatrix} := \mathbf{h}(\mathbf{x}_{\mathbf{S}_k}) \tag{6}$$

where ${}^{J_k}_{G}\boldsymbol{\theta} := \mathrm{Log}({}^{J_k}_{G}\mathbf{R})$ and $\mathrm{Log}(\cdot)$ is the SO(3) matrix logarithmic function [4]. Eq. (6) can be linearized at the state estimate $\hat{\mathbf{x}}_{\mathbf{S}_k}$ as:

$$\tilde{\mathbf{z}}_{\mathbf{S}_k} := \mathbf{z}_{\mathbf{S}_k} - \mathbf{h}(\hat{\mathbf{x}}_{\mathbf{S}_k}) = \mathbf{H}_{\mathbf{S}_k}\tilde{\mathbf{x}}_{\mathbf{S}_k} \tag{7}$$

where $\mathbf{H}_{\mathbf{S}_k}$ is the measurement Jacobian matrix:

$$\mathbf{H}_{\mathbf{S}_k} = \begin{bmatrix} \frac{\partial {}^{J_k}_{G}\boldsymbol{\theta}}{\partial {}^{I_k}_{G}\boldsymbol{\theta}} & \frac{\partial {}^{J_k}_{G}\boldsymbol{\theta}}{\partial {}^{G}\mathbf{p}_{I_k}} & \frac{\partial {}^{J_k}_{G}\boldsymbol{\theta}}{\partial {}^{J}_{I}\boldsymbol{\theta}} & \frac{\partial {}^{J_k}_{G}\boldsymbol{\theta}}{\partial {}^{J}\mathbf{p}_{I}} & \frac{\partial {}^{J_k}_{G}\boldsymbol{\theta}}{\partial {}^{J}t_I} \\ \frac{\partial {}^{G}\mathbf{p}_{J_k}}{\partial {}^{I_k}_{G}\boldsymbol{\theta}} & \frac{\partial {}^{G}\mathbf{p}_{J_k}}{\partial {}^{G}\mathbf{p}_{I_k}} & \frac{\partial {}^{G}\mathbf{p}_{J_k}}{\partial {}^{J}_{I}\boldsymbol{\theta}} & \frac{\partial {}^{G}\mathbf{p}_{J_k}}{\partial {}^{J}\mathbf{p}_{I}} & \frac{\partial {}^{G}\mathbf{p}_{J_k}}{\partial {}^{J}t_I} \end{bmatrix} \tag{8}$$

$$= \begin{bmatrix} {}^{J}_{I}\mathbf{R} & \mathbf{0}_3 & \mathbf{I}_3 & \mathbf{0}_3 & {}^{J}_{I}\mathbf{R}\,{}^{I_k}\boldsymbol{\omega}_{I_k} \\ -{}^{G}_{I_k}\mathbf{R}\lfloor {}^{I}\mathbf{p}_J \rfloor & \mathbf{I}_3 & -{}^{G}_{I_k}\mathbf{R}\lfloor {}^{I}\mathbf{p}_J \rfloor {}^{I}_{J}\mathbf{R} & -{}^{G}_{I_k}\mathbf{R}\,{}^{I}_{J}\mathbf{R} & {}^{G}\mathbf{v}_{I_k} - {}^{G}_{I_k}\mathbf{R}\lfloor {}^{I}\mathbf{p}_J \rfloor {}^{I_k}\boldsymbol{\omega}_{I_k} \end{bmatrix} \tag{9}$$

2.4 Observability Matrix

The observability matrix for the linearized system is [5]:

$$\mathbf{M_S} = \begin{bmatrix} \mathbf{H_{S_0}} \\ \mathbf{H_{S_1}}\mathbf{\Phi_S}(t_1,t_0) \\ \vdots \\ \mathbf{H_{S_k}}\mathbf{\Phi_S}(t_k,t_0) \\ \vdots \end{bmatrix} \tag{10}$$

For any $k > 1$, the k-th block row, $\mathbf{M_{S_k}}$ can be derived as [see Eq. (5) and (9)]:

$$\mathbf{M_{S_k}} := \mathbf{H_{S_k}}\mathbf{\Phi_S}(t_k,t_0) \tag{11}$$

$$= \begin{bmatrix} {}^{J}_{I}\mathbf{R}\,{}^{I_k}_{I_0}\mathbf{R} & \mathbf{0}_3 & \mathbf{I}_3 & \mathbf{0}_3 & {}^{J}_{I}\mathbf{R}\,{}^{I_k}\boldsymbol{\omega}_{I_k} \\ -{}^{G}_{I_k}\mathbf{R}\lfloor {}^{I}\mathbf{p}_J \rfloor {}^{I_k}_{I_0}\mathbf{R} - {}^{G}_{I_0}\mathbf{R}\lfloor {}^{I_0}\mathbf{p}_{I_k} \rfloor & \mathbf{I}_3 & -{}^{G}_{I_k}\mathbf{R}\lfloor {}^{I}\mathbf{p}_J \rfloor {}^{I}_{J}\mathbf{R} & -{}^{G}_{I_k}\mathbf{R}\,{}^{I}_{J}\mathbf{R} & {}^{G}\mathbf{v}_{I_k} - {}^{G}_{I_k}\mathbf{R}\lfloor {}^{I}\mathbf{p}_J \rfloor {}^{I_k}\boldsymbol{\omega}_{I_k} \end{bmatrix} \tag{12}$$

If we can find matrix $\mathbf{N}$ that satisfies $\mathbf{M_{S_k}}\mathbf{N} = \mathbf{0}$ $, \forall k > 1$, the basis of $\mathbf{N}$ indicate the unobservable directions of the linearized system.

2.4.1 General Motion

Lemma 2.1. *If the system undergoes general 3D motion with fully exited more than 1 axis rotation, the state is fully observable.*

Numerical Study: The state estimation with online calibration shows consistent estimation results under general 3D motion.

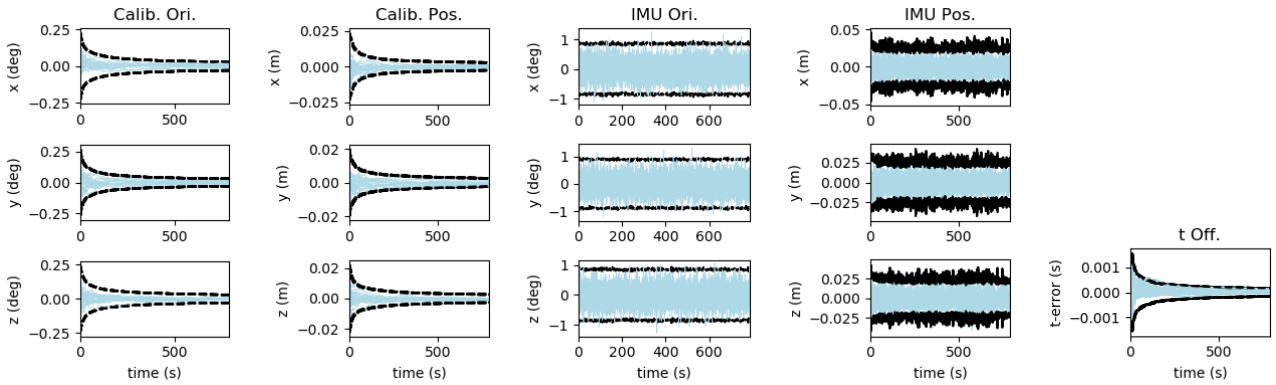

Figure 4: State estimation with online calibration performance across 20 Monte-Carlo simulations where the blue lines are the estimation error and black lines indicate the $\pm 3\sigma$ bounds

2.5 Degenerate Motion Analysis

By analyzing the observability matrix $\mathbf{M}_{\mathbf{S}_k}$, we identify the following degenerate motions that cause the state to be partially unobservable.

2.5.1 1-Axis Rotation and General 3-Axis Translation Motion

Lemma 2.2. *If the system undergoes 1-axis rotation and general 3-axis translation motion, the state is partially unobservable with directions as:*

$$\mathbf{N} = \begin{bmatrix} \mathbf{0}_{3\times 1} \\ \mathbf{k} \\ \mathbf{0}_{3\times 1} \\ {}^{J}_{I}\mathbf{R}\mathbf{k} \\ 0 \end{bmatrix} \tag{13}$$

where $\mathbf{k}$ *is the rotation axis. The relevant parameters are:* ${}^{G}\mathbf{p}_{I_k}$, ${}^{J}\mathbf{p}_{I}$.

Proof. The motion constraint can be interpreted as the following geometric constraints:

$${}^{I_0}_{G}\mathbf{R}\mathbf{k} = {}^{I_k}_{G}\mathbf{R}\mathbf{k} = \mathbf{k} \tag{14}$$

We can find $\mathbf{N}$ is the null space of $\mathbf{M}_{\mathbf{S}_k}$ with the above constraints:

$$\mathbf{M}_{\mathbf{S}_k}\mathbf{N} = \begin{bmatrix} \mathbf{0}_{3\times 1} \\ \mathbf{k} - {}^{G}_{I_k}\mathbf{R}^{I}_{J}\mathbf{R}^{J}_{I}\mathbf{R}\mathbf{k} \end{bmatrix} = \mathbf{0}_{6\times 1} \tag{15}$$

This completes the proof. □

Numerical Study: The state estimation with online calibration shows inconsistent estimation results under 1-axis rotation and general 3-axis translation motion. Specifically, we have the following values from simulation:

$$\mathbf{k} = \begin{bmatrix} 0 \\ 0 \\ 1 \end{bmatrix}, {}^{J}_{I}\mathbf{R}\mathbf{k} = \begin{bmatrix} 0 \\ 0 \\ 1 \end{bmatrix} \tag{16}$$

which makes the z-axis of position estimation of both calibration and robot pose partially unobservable.

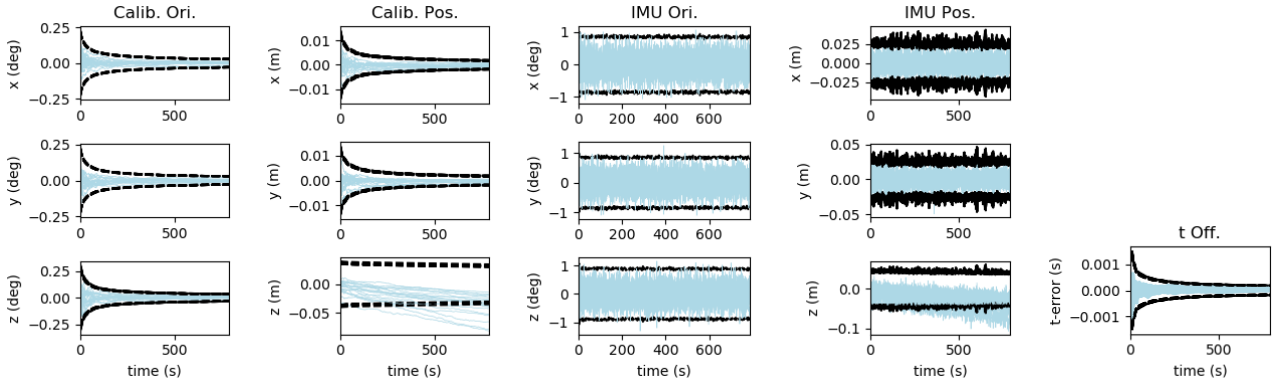

Figure 5: State estimation with online calibration performance across 20 Monte-Carlo simulations where the blue lines are the estimation error and black lines indicate the $\pm 3\sigma$ bounds

2.5.2 Constant Local Angular and Linear Velocity Motion

Lemma 2.3. *If the system undergoes constant local angular and linear velocity motion, the state is partially unobservable with directions as:*

$$\mathbf{N} = \begin{bmatrix} \mathbf{N}_1 & \mathbf{N}_2 \end{bmatrix} = \begin{bmatrix} \mathbf{0}_{3\times 1} & \mathbf{0}_{3\times 1} \\ \mathbf{k} & \mathbf{0}_{3\times 1} \\ \mathbf{0}_{3\times 1} & -{}^{J}_{I}\mathbf{R}^{I_0}\boldsymbol{\omega}_{I_0} \\ {}^{J}_{I}\mathbf{R}\mathbf{k} & {}^{J}_{I}\mathbf{R}^{I_0}\mathbf{v}_{I_0} \\ 0 & 1 \end{bmatrix} \tag{17}$$

where $\mathbf{k}$ *is the angular velocity axis of rotation. The relevant parameters are:* ${}^{G}\mathbf{p}_{I_k}$, ${}^{J}_{I}\bar{q}$, ${}^{J}\mathbf{p}_{I}, {}^{J}t_{I}$.

Proof. The motion constraint can be interpreted as the following geometric constraints:

$${}^{I_0}_{G}\mathbf{R}\mathbf{k} = {}^{I_k}_{G}\mathbf{R}\mathbf{k} = \mathbf{k}, \quad {}^{I_k}\mathbf{v}_{I_k} = {}^{I_0}\mathbf{v}_{I_0}, \quad {}^{I_k}\boldsymbol{\omega}_{I_k} = {}^{I_0}\boldsymbol{\omega}_{I_0} \tag{18}$$

By applying the above constraints, $\mathbf{N}$ become the null space of $\mathbf{M}_{\mathbf{S}_k}$ (only showing the new directions):

$$\mathbf{M}_{\mathbf{S}_k}\mathbf{N}_2 = \begin{bmatrix} -{}^{J}_{I}\mathbf{R}^{I_0}\boldsymbol{\omega}_{I_0} + {}^{J}_{I}\mathbf{R}^{I_k}\boldsymbol{\omega}_{I_k} \\ {}^{G}_{I_k}\mathbf{R}\lfloor {}^{I}\mathbf{p}_{J} \rfloor {}^{I}_{J}\mathbf{R}{}^{J}_{I}\mathbf{R}^{I_0}\boldsymbol{\omega}_{I_0} - {}^{G}_{I_k}\mathbf{R}^{I}_{J}\mathbf{R}{}^{J}_{I}\mathbf{R}^{I_0}\mathbf{v}_{I_0} + {}^{G}\mathbf{v}_{I_k} - {}^{G}_{I_k}\mathbf{R}\lfloor {}^{I}\mathbf{p}_{J} \rfloor {}^{I_k}\boldsymbol{\omega}_{I_k} \end{bmatrix} = \mathbf{0}_{6\times 1} \tag{19}$$

This completes the proof. □

Numerical Study: The state estimation with online calibration shows inconsistent estimation results under constant local angular and linear velocity motion. Specifically, we have the following values from simulation:

$$\mathbf{k} = \begin{bmatrix} 0 \\ 0 \\ 1 \end{bmatrix}, {}^{J}_{I}\mathbf{R} = \begin{bmatrix} 1 & 0 & 0 \\ 0 & 1 & 0 \\ 0 & 0 & 1 \end{bmatrix}, {}^{I_0}\boldsymbol{\omega}_{I_0} = \begin{bmatrix} 0 \\ 0 \\ 1 \end{bmatrix}, {}^{I_0}\mathbf{v}_{I_0} = \begin{bmatrix} 2 \\ 0 \\ 0 \end{bmatrix} \tag{20}$$

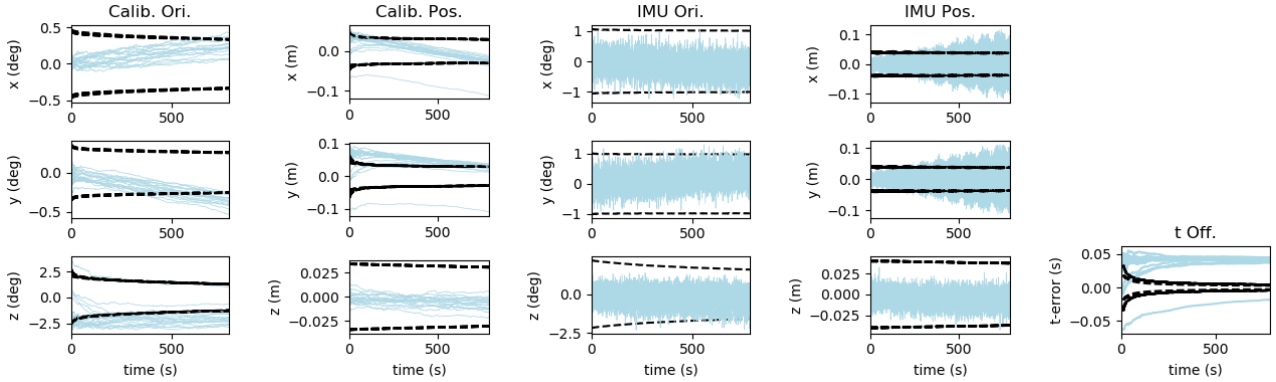

Figure 6: State estimation with online calibration performance across 20 Monte-Carlo simulations where the blue lines are the estimation error and black lines indicate the $\pm 3\sigma$ bounds

2.5.3 3-Axis or 2-Axis Translation without Rotation Motion

Lemma 2.4. *If the system undergoes pure 3D translation or 2D translation (planar) motion, the state is partially unobservable with directions as:*

$$\mathbf{N} = \begin{bmatrix} \mathbf{0}_3 \\ \mathbf{I} \\ \mathbf{0}_3 \\ {}^{J}_{I}\mathbf{R}\,{}^{I_0}_{G}\mathbf{R} \\ \mathbf{0}_{1\times 3} \end{bmatrix} \tag{21}$$

The relevant parameters are: ${}^{G}\mathbf{p}_{I_k}$, ${}^{J}\mathbf{p}_{I}$.

Proof. The motion constraint can be interpreted as the following geometric constraints:

$${}^{I_0}_{G}\mathbf{R} = {}^{I_k}_{G}\mathbf{R}, \qquad {}^{I_k}\boldsymbol{\omega}_{I_k} = {}^{I_0}\boldsymbol{\omega}_{I_0} = \mathbf{0}_{3\times 1} \tag{22}$$

The observability matrix can be rewritten with constraints as:

$$\begin{aligned} \mathbf{M}_{\mathbf{S}_k} &= \begin{bmatrix} {}^{J}_{I}\mathbf{R}\,{}^{I_k}_{I_0}\mathbf{R} & \mathbf{0}_3 & \mathbf{I}_3 & \mathbf{0}_3 & {}^{J}_{I}\mathbf{R}\,{}^{I_k}\boldsymbol{\omega}_{I_k} \\ -{}^{G}_{I_k}\mathbf{R}\lfloor {}^{I}\mathbf{p}_J \rfloor {}^{I_k}_{I_0}\mathbf{R} - {}^{G}_{I_0}\mathbf{R}\lfloor {}^{I_0}\mathbf{p}_{I_k} \rfloor & \mathbf{I}_3 & -{}^{G}_{I_k}\mathbf{R}\lfloor {}^{I}\mathbf{p}_J \rfloor {}^{I}_{J}\mathbf{R} & -{}^{G}_{I_k}\mathbf{R}\,{}^{I}_{J}\mathbf{R} & {}^{G}\mathbf{v}_{I_k} - {}^{G}_{I_k}\mathbf{R}\lfloor {}^{I}\mathbf{p}_J \rfloor {}^{I_k}\boldsymbol{\omega}_{I_k} \end{bmatrix} \\ &= \begin{bmatrix} {}^{J}_{I}\mathbf{R} & \mathbf{0}_3 & \mathbf{I}_3 & \mathbf{0}_3 & \mathbf{0}_{3\times 1} \\ -{}^{G}_{I_k}\mathbf{R}\lfloor {}^{I}\mathbf{p}_J \rfloor - {}^{G}_{I_0}\mathbf{R}\lfloor {}^{I_0}\mathbf{p}_{I_k} \rfloor & \mathbf{I}_3 & -{}^{G}_{I_k}\mathbf{R}\lfloor {}^{I}\mathbf{p}_J \rfloor {}^{I}_{J}\mathbf{R} & -{}^{G}_{I_k}\mathbf{R}\,{}^{I}_{J}\mathbf{R} & {}^{G}\mathbf{v}_{I_k} \end{bmatrix} \end{aligned} \tag{23}$$

By applying the above constraints, $\mathbf{N}$ become the null space of $\mathbf{M}_{\mathbf{S}_k}$:

$$\mathbf{M}_{\mathbf{S}_k}\mathbf{N} = \begin{bmatrix} \mathbf{0}_3 \\ \mathbf{I}_3 - {}^{G}_{I_k}\mathbf{R}\,{}^{I}_{J}\mathbf{R}\,{}^{J}_{I}\mathbf{R}\,{}^{I_0}_{G}\mathbf{R} \end{bmatrix} = \mathbf{0}_{6\times 1} \tag{24}$$

This completes the proof. □

Numerical Study: The state estimation with online calibration shows inconsistent estimation results under pure 3D translation motion. Specifically, we have the following values from simulation:

$${}^{J}_{I}\mathbf{R}\,{}^{I_0}_{G}\mathbf{R} = \begin{bmatrix} 1 & 0 & 0 \\ 0 & 1 & 0 \\ 0 & 0 & 1 \end{bmatrix} \tag{25}$$

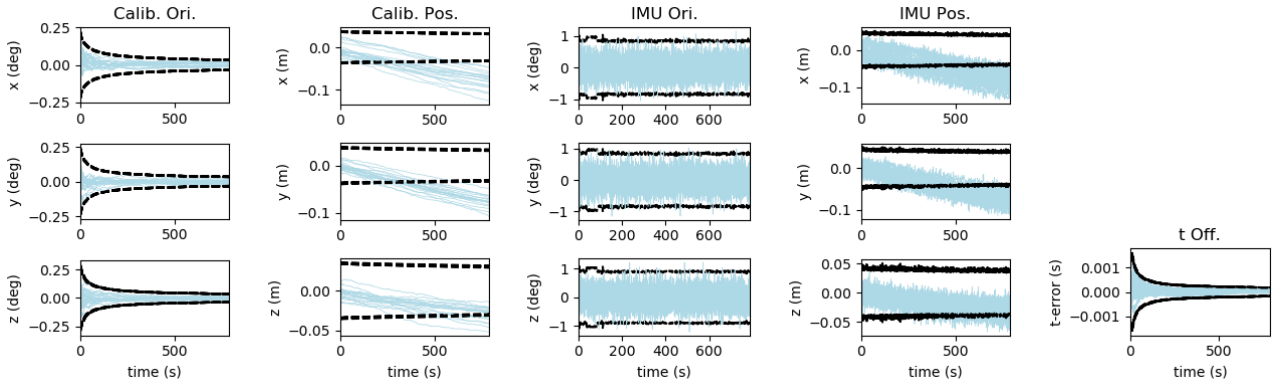

Figure 7: State estimation with online calibration performance across 20 Monte-Carlo simulations where the blue lines are the estimation error and black lines indicate the $\pm 3\sigma$ bounds

2.5.4 1-Axis Translation without Rotation Motion

Lemma 2.5. *If the system undergoes general local 1-axis translation (straight line motion with general velocity) without rotation, the state is partially unobservable with directions as:*

$$\mathbf{N} = \begin{bmatrix} \mathbf{N}_1 & \mathbf{N}_2 \end{bmatrix} = \begin{bmatrix} \mathbf{k} & \mathbf{0}_3 \\ \mathbf{0}_{3\times 1} & \mathbf{I}_3 \\ -{}^J_I\mathbf{R}\mathbf{k} & \mathbf{0}_3 \\ \mathbf{0}_{3\times 1} & {}^J_I\mathbf{R}\,{}^{I_0}_G\mathbf{R} \\ 0 & \mathbf{0}_{1\times 3} \end{bmatrix} \tag{26}$$

where $\mathbf{k}$ *is the axis of the translation. The relevant parameters are:* ${}^{I_k}_G\bar{q}$, ${}^G\mathbf{p}_{I_k}$, ${}^J_I\bar{q}$, ${}^J\mathbf{p}_I$.

Proof. The motion constraint can be interpreted as the following geometric constraints:

$${}^{I_0}_G\mathbf{R} = {}^{I_k}_G\mathbf{R}, \quad {}^{I_k}\boldsymbol{\omega}_{I_k} = {}^{I_0}\boldsymbol{\omega}_{I_0} = \mathbf{0}_{3\times 1}, \quad {}^{I_0}\mathbf{p}_{I_k} = f(t_k)\mathbf{k} \tag{27}$$

where $f(\cdot)$ is a scalar function.

The observability matrix can be rewritten with constraints as:

$$\mathbf{M}_{\mathbf{S}_k} = \begin{bmatrix} {}^J_I\mathbf{R}\,{}^{I_k}_{I_0}\mathbf{R} & \mathbf{0}_3 & \mathbf{I}_3 & \mathbf{0}_3 & {}^J_I\mathbf{R}\,{}^{I_k}\boldsymbol{\omega}_{I_k} \\ -{}^G_{I_k}\mathbf{R}\lfloor {}^I\mathbf{p}_J\rfloor\,{}^{I_k}_{I_0}\mathbf{R} - {}^G_{I_0}\mathbf{R}\lfloor {}^{I_0}\mathbf{p}_{I_k}\rfloor & \mathbf{I}_3 & -{}^G_{I_k}\mathbf{R}\lfloor {}^I\mathbf{p}_J\rfloor\,{}^I_J\mathbf{R} & -{}^G_{I_k}\mathbf{R}\,{}^I_J\mathbf{R} & {}^G\mathbf{v}_{I_k} - {}^G_{I_k}\mathbf{R}\lfloor {}^I\mathbf{p}_J\rfloor\,{}^{I_k}\boldsymbol{\omega}_{I_k} \end{bmatrix} \tag{28}$$

$$= \begin{bmatrix} {}^J_I\mathbf{R} & \mathbf{0}_3 & \mathbf{I}_3 & \mathbf{0}_3 & \mathbf{0}_{3\times 1} \\ -{}^G_{I_0}\mathbf{R}\lfloor {}^I\mathbf{p}_J\rfloor - {}^G_{I_0}\mathbf{R}\lfloor f(t_k)\mathbf{k}\rfloor & \mathbf{I}_3 & -{}^G_{I_0}\mathbf{R}\lfloor {}^I\mathbf{p}_J\rfloor\,{}^I_J\mathbf{R} & -{}^G_{I_0}\mathbf{R}\,{}^I_J\mathbf{R} & {}^G\mathbf{v}_{I_k} \end{bmatrix} \tag{29}$$

By applying the above constraint, $\mathbf{N}$ become the null space of $\mathbf{M}_{\mathbf{S}_k}$:

$$\mathbf{M}_{\mathbf{S}_k}\mathbf{N}_1 = \begin{bmatrix} {}^J_I\mathbf{R}\mathbf{k} - {}^J_I\mathbf{R}\mathbf{k} \\ -{}^G_{I_0}\mathbf{R}\lfloor {}^I\mathbf{p}_J\rfloor\mathbf{k} - {}^G_{I_0}\mathbf{R}\lfloor f(t_k)\mathbf{k}\rfloor\mathbf{k} + {}^G_{I_0}\mathbf{R}\lfloor {}^I\mathbf{p}_J\rfloor\,{}^I_J\mathbf{R}\,{}^J_I\mathbf{R}\mathbf{k} \end{bmatrix} = \begin{bmatrix} \mathbf{0}_{3\times 1} \\ -{}^G_{I_0}\mathbf{R}\lfloor f(t_k)\mathbf{k}\rfloor\mathbf{k} \end{bmatrix} = \mathbf{0}_{6\times 1} \tag{30}$$

$$\mathbf{M}_{\mathbf{S}_k}\mathbf{N}_2 = \begin{bmatrix} \mathbf{0}_3 \\ \mathbf{I}_3 - {}^G_{I_0}\mathbf{R}\,{}^I_J\mathbf{R}\,{}^J_I\mathbf{R}\,{}^{I_0}_G\mathbf{R} \end{bmatrix} = \mathbf{0}_{6\times 3} \tag{31}$$

This completes the proof. □

Numerical Study: The state estimation with online calibration shows inconsistent estimation results under general local 1-axis translation (straight line motion with general velocity) without rotation. Specifically, we have the following values from simulation:

$$\mathbf{k} = \begin{bmatrix} 0 \\ 0 \\ 1 \end{bmatrix}, {}^J_I\mathbf{R}\mathbf{k} = \begin{bmatrix} 0 \\ 0 \\ 1 \end{bmatrix}, {}^J_I\mathbf{R}\,{}^{I_0}_G\mathbf{R} = \begin{bmatrix} 1 & 0 & 0 \\ 0 & 1 & 0 \\ 0 & 0 & 1 \end{bmatrix} \tag{32}$$

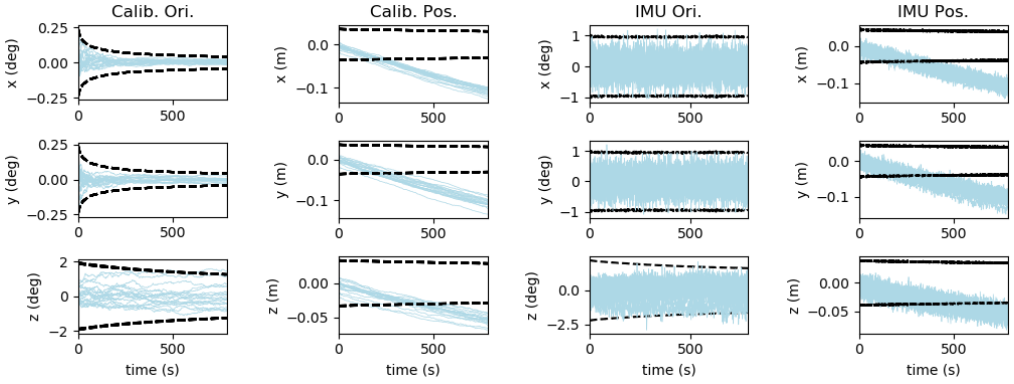

Figure 8: State estimation with online calibration performance across 20 Monte-Carlo simulations where the blue lines are the estimation error and black lines indicate the $\pm 3\sigma$ bounds

2.5.5 Constant Velocity 1-Axis Translation without Rotation Motion

Lemma 2.6. *If the system undergoes constant local linear velocity motion (straight line motion with constant velocity) without rotation, the state is partially unobservable with directions as:*

$$\mathbf{N} = \begin{bmatrix} \mathbf{N}_1 & \mathbf{N}_2 & \mathbf{N}_3 \end{bmatrix} = \begin{bmatrix} \mathbf{k} & \mathbf{0}_3 & \mathbf{0}_{3\times 1} \\ \mathbf{0}_{3\times 1} & \mathbf{I}_3 & -{}^{G}\mathbf{v}_{I_0} \\ -{}^{J}_{I}\mathbf{R}\mathbf{k} & \mathbf{0}_3 & \mathbf{0}_{3\times 1} \\ \mathbf{0}_{3\times 1} & {}^{J}_{I}\mathbf{R}\,{}^{I_0}_{G}\mathbf{R} & \mathbf{0}_{3\times 1} \\ 0 & \mathbf{0}_{1\times 3} & 1 \end{bmatrix} \tag{33}$$

where $\mathbf{k}$ *is the axis of the translation. The relevant parameters are:* ${}^{I_k}_{G}\bar{q}$, ${}^{G}\mathbf{p}_{I_k}$, ${}^{J}_{I}\bar{q}$, ${}^{J}\mathbf{p}_{I}$, ${}^{J}t_{I}$.

Proof. The motion constraint can be interpreted as the following geometric constraints:

$${}^{I_0}_{G}\mathbf{R} = {}^{I_k}_{G}\mathbf{R}, \quad {}^{I_k}\boldsymbol{\omega}_{I_k} = {}^{I_0}\boldsymbol{\omega}_{I_0} = \mathbf{0}_{3\times 1}, \quad {}^{I_0}\mathbf{p}_{I_k} = f(t_k)\mathbf{k}, \quad {}^{I_k}\mathbf{v}_{I_k} = {}^{I_0}\mathbf{v}_{I_0} = s\mathbf{k} \tag{34}$$

where $f(\cdot)$ is a scalar function and s is the speed of the motion. The observability matrix can be rewritten with constraints as:

$$\mathbf{M}_{\mathbf{S}_k} = \begin{bmatrix} {}^{J}_{I}\mathbf{R}\,{}^{I_k}_{I_0}\mathbf{R} & \mathbf{0}_3 & \mathbf{I}_3 & \mathbf{0}_3 & {}^{J}_{I}\mathbf{R}\,{}^{I_k}\boldsymbol{\omega}_{I_k} \\ -{}^{G}_{I_k}\mathbf{R}\lfloor {}^{I}\mathbf{p}_{J}\rfloor\,{}^{I_k}_{I_0}\mathbf{R} - {}^{G}_{I_0}\mathbf{R}\lfloor {}^{I_0}\mathbf{p}_{I_k}\rfloor & \mathbf{I}_3 & -{}^{G}_{I_k}\mathbf{R}\lfloor {}^{I}\mathbf{p}_{J}\rfloor\,{}^{I}_{J}\mathbf{R} & -{}^{G}_{I_k}\mathbf{R}\,{}^{I}_{J}\mathbf{R} & {}^{G}\mathbf{v}_{I_k} - {}^{G}_{I_k}\mathbf{R}\lfloor {}^{I}\mathbf{p}_{J}\rfloor\,{}^{I_k}\boldsymbol{\omega}_{I_k} \end{bmatrix} \tag{35}$$

$$= \begin{bmatrix} {}^{J}_{I}\mathbf{R} & \mathbf{0}_3 & \mathbf{I}_3 & \mathbf{0}_3 & \mathbf{0}_{3\times 1} \\ -{}^{G}_{I_0}\mathbf{R}\lfloor {}^{I}\mathbf{p}_{J}\rfloor - {}^{G}_{I_0}\mathbf{R}\lfloor {}^{I_0}\mathbf{p}_{I_k}\rfloor & \mathbf{I}_3 & -{}^{G}_{I_0}\mathbf{R}\lfloor {}^{I}\mathbf{p}_{J}\rfloor\,{}^{I}_{J}\mathbf{R} & -{}^{G}_{I_0}\mathbf{R}\,{}^{I}_{J}\mathbf{R} & {}^{G}\mathbf{v}_{I_0} \end{bmatrix} \tag{36}$$

By applying the above constraint, $\mathbf{N}$ become the null space of $\mathbf{M}_{\mathbf{S}_k}$ (only showing the new directions):

$$\mathbf{M}_{\mathbf{S}_k}\mathbf{N}_3 = \begin{bmatrix} \mathbf{0}_{3\times 1} \\ -{}^{G}\mathbf{v}_{I_0} + {}^{G}\mathbf{v}_{I_k} \end{bmatrix} = \begin{bmatrix} \mathbf{0}_{3\times 1} \\ -{}^{G}_{I_0}\mathbf{R}\,{}^{I_0}\mathbf{v}_{I_0} + {}^{G}_{I_k}\mathbf{R}\,{}^{I_k}\mathbf{v}_{I_k} \end{bmatrix} = \mathbf{0}_{6\times 1} \tag{37}$$

This completes the proof. □

Numerical Study: The state estimation with online calibration shows inconsistent estimation results under constant local linear velocity motion (straight line motion with constant velocity) without rotation. Specifically, we have the following values from simulation:

$$\mathbf{k} = \begin{bmatrix} 0 \\ 0 \\ 1 \end{bmatrix}, {}^{J}_{I}\mathbf{R}\,{}^{I_0}_{G}\mathbf{R} = \begin{bmatrix} 1 & 0 & 0 \\ 0 & 1 & 0 \\ 0 & 0 & 1 \end{bmatrix}, {}^{G}\mathbf{v}_{I_0} = \begin{bmatrix} 0 \\ 0 \\ 0.1 \end{bmatrix} \tag{38}$$

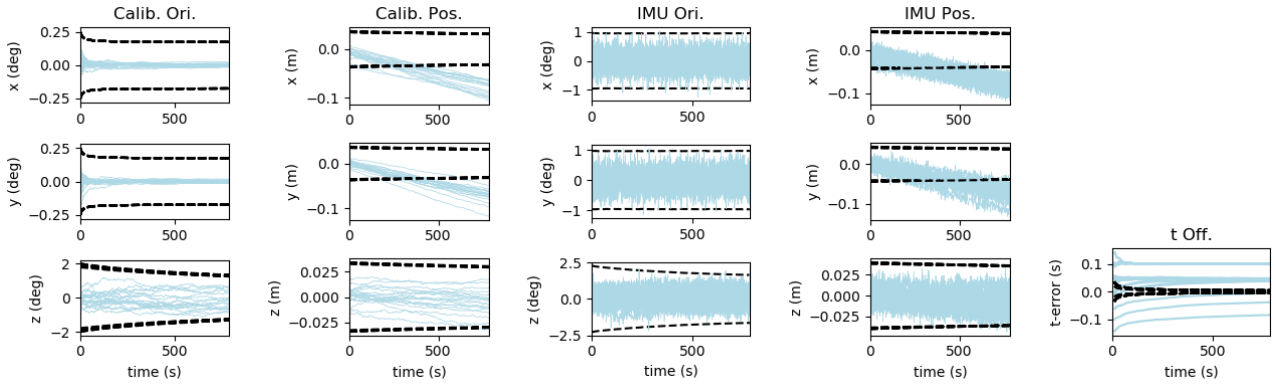

Figure 9: State estimation with online calibration performance across 20 Monte-Carlo simulations where the blue lines are the estimation error and black lines indicate the $\pm 3\sigma$ bounds

2.5.6 1-Axis Rotation without Translation Motion

Lemma 2.7. *If the system undergoes general local 1-axis rotation without translation, the state is partially unobservable with directions as:*

$$\mathbf{N} = \begin{bmatrix} \mathbf{N}_1 & \mathbf{N}_2 \end{bmatrix} = \begin{bmatrix} \mathbf{k} & \mathbf{0}_{3\times1} \\ \mathbf{0}_{3\times1} & \mathbf{k} \\ -{}^{J}_{I}\mathbf{R}\mathbf{k} & \mathbf{0}_{3\times1} \\ \mathbf{0}_{3\times1} & {}^{J}_{I}\mathbf{R}\mathbf{k} \\ 0 & 0 \end{bmatrix} \tag{39}$$

where $\mathbf{k}$ *is the rotation axis. The relevant parameters are:* ${}^{I_k}_{G}\bar{q}$, ${}^{G}\mathbf{p}_{I_k}$, ${}^{J}_{I}\bar{q}$, ${}^{J}\mathbf{p}_{I}$.

Proof. The motion constraint can be interpreted as the following geometric constraints:

$${}^{I_0}_{G}\mathbf{R}\mathbf{k} = {}^{I_k}_{G}\mathbf{R}\mathbf{k} = \mathbf{k}, \quad {}^{I_0}\mathbf{p}_{I_k} = \mathbf{0}_{3\times1}, \quad {}^{I_k}\mathbf{v}_{I_k} = {}^{I_0}\mathbf{v}_{I_0} = \mathbf{0}_{3\times1} \tag{40}$$

The observability matrix can be rewritten with constraints as:

$$\mathbf{M}_{\mathbf{S}_k} = \begin{bmatrix} {}^{J}_{I}\mathbf{R}\,{}^{I_k}_{I_0}\mathbf{R} & \mathbf{0}_3 & \mathbf{I}_3 & \mathbf{0}_3 & {}^{J}_{I}\mathbf{R}\,{}^{I_k}\boldsymbol{\omega}_{I_k} \\ -{}^{G}_{I_k}\mathbf{R}\lfloor {}^{I}\mathbf{p}_J \rfloor {}^{I_k}_{I_0}\mathbf{R} - {}^{G}_{I_0}\mathbf{R}\lfloor {}^{I_0}\mathbf{p}_{I_k} \rfloor & \mathbf{I}_3 & -{}^{G}_{I_k}\mathbf{R}\lfloor {}^{I}\mathbf{p}_J \rfloor {}^{I}_{J}\mathbf{R} & -{}^{G}_{I_k}\mathbf{R}\,{}^{I}_{J}\mathbf{R} & {}^{G}\mathbf{v}_{I_k} - {}^{G}_{I_k}\mathbf{R}\lfloor {}^{I}\mathbf{p}_J \rfloor {}^{I_k}\boldsymbol{\omega}_{I_k} \end{bmatrix} \tag{41}$$

$$= \begin{bmatrix} {}^{J}_{I}\mathbf{R}\,{}^{I_k}_{I_0}\mathbf{R} & \mathbf{0}_3 & \mathbf{I}_3 & \mathbf{0}_3 & {}^{J}_{I}\mathbf{R}\,{}^{I_k}\boldsymbol{\omega}_{I_k} \\ -{}^{G}_{I_k}\mathbf{R}\lfloor {}^{I}\mathbf{p}_J \rfloor {}^{I_k}_{I_0}\mathbf{R} & \mathbf{I}_3 & -{}^{G}_{I_k}\mathbf{R}\lfloor {}^{I}\mathbf{p}_J \rfloor {}^{I}_{J}\mathbf{R} & -{}^{G}_{I_k}\mathbf{R}\,{}^{I}_{J}\mathbf{R} & -{}^{G}_{I_k}\mathbf{R}\lfloor {}^{I}\mathbf{p}_J \rfloor {}^{I_k}\boldsymbol{\omega}_{I_k} \end{bmatrix} \tag{42}$$

By applying the above constraint, $\mathbf{N}$ become the null space of $\mathbf{M}_{\mathbf{S}_k}$:

$$\mathbf{M}_{\mathbf{S}_k}\mathbf{N}_1 = \begin{bmatrix} {}^{J}_{I}\mathbf{R}\,{}^{I_k}_{I_0}\mathbf{R}\mathbf{k} - {}^{J}_{I}\mathbf{R}\mathbf{k} \\ -{}^{G}_{I_k}\mathbf{R}\lfloor {}^{I}\mathbf{p}_J \rfloor {}^{I_k}_{I_0}\mathbf{R}\mathbf{k} + {}^{G}_{I_k}\mathbf{R}\lfloor {}^{I}\mathbf{p}_J \rfloor {}^{I}_{J}\mathbf{R}\,{}^{J}_{I}\mathbf{R}\mathbf{k} \end{bmatrix} = \mathbf{0}_{6\times1} \tag{43}$$

$$\mathbf{M}_{\mathbf{S}_k}\mathbf{N}_2 = \begin{bmatrix} \mathbf{0}_{3\times1} \\ \mathbf{k} - {}^{G}_{I_k}\mathbf{R}\,{}^{I}_{J}\mathbf{R}\,{}^{J}_{I}\mathbf{R}\mathbf{k} \end{bmatrix} = \mathbf{0}_{6\times1} \tag{44}$$

This completes the proof. □

Numerical Study: The state estimation with online calibration shows inconsistent estimation results under local 1-axis rotation without translation. Specifically, we have the following values from simulation:

$$\mathbf{k} = \begin{bmatrix} 0 \\ 0 \\ 1 \end{bmatrix}, {}^{J}_{I}\mathbf{R}\mathbf{k} = \begin{bmatrix} 0 \\ 0 \\ 1 \end{bmatrix} \tag{45}$$

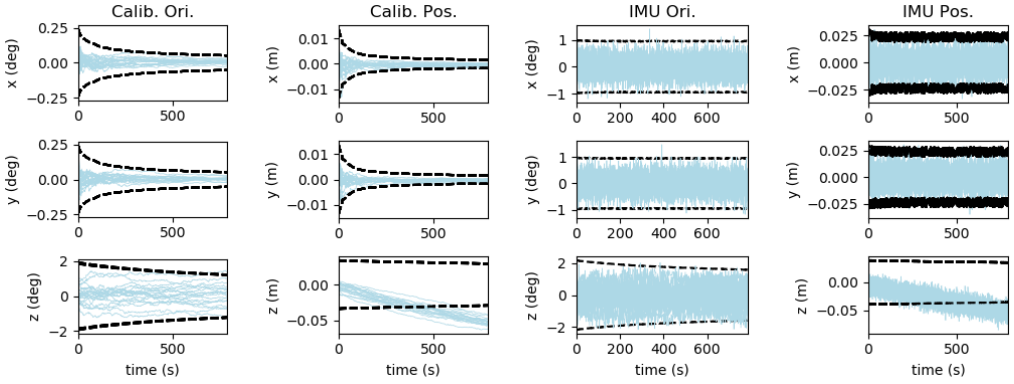

Figure 10: State estimation with online calibration performance across 20 Monte-Carlo simulations where the blue lines are the estimation error and black lines indicate the $\pm 3\sigma$ bounds

2.5.7 Constant Velocity 1-Axis Rotation without Translation Motion

Lemma 2.8. *If the system undergoes constant local 1-axis angular velocity motion without translation, the state is partially unobservable with directions as:*

$$\mathbf{N} = \begin{bmatrix} \mathbf{N}_1 & \mathbf{N}_2 & \mathbf{N}_3 \end{bmatrix} = \begin{bmatrix} \mathbf{k} & \mathbf{0}_{3\times1} & -{}^{I_0}\boldsymbol{\omega}_{I_0} \\ \mathbf{0}_{3\times1} & \mathbf{k} & \mathbf{0}_{3\times1} \\ -{}^{J}_{I}\mathbf{R}\mathbf{k} & \mathbf{0}_{3\times1} & \mathbf{0}_{3\times1} \\ \mathbf{0}_{3\times1} & {}^{J}_{I}\mathbf{R}\mathbf{k} & \mathbf{0}_{3\times1} \\ 0 & 0 & 1 \end{bmatrix} \tag{46}$$

where $\mathbf{k}$ *is the rotation axis. The relevant parameters are:* ${}^{I_k}_{G}\bar{q}$, ${}^{G}\mathbf{p}_{I_k}$, ${}^{J}_{I}\bar{q}$, ${}^{J}\mathbf{p}_{I}$, ${}^{J}t_{I}$.

Proof. The motion constraint can be interpreted as the following geometric constraints:

$${}^{I_0}_{G}\mathbf{R}\mathbf{k} = {}^{I_k}_{G}\mathbf{R}\mathbf{k} = \mathbf{k}, \quad {}^{I_0}\mathbf{p}_{I_k} = \mathbf{0}_{3\times1}, \quad {}^{I_k}\mathbf{v}_{I_k} = {}^{I_0}\mathbf{v}_{I_0} = \mathbf{0}_{3\times1}, \quad {}^{I_k}\boldsymbol{\omega}_{I_k} = {}^{I_0}\boldsymbol{\omega}_{I_0} = s\mathbf{k} \tag{47}$$

where s is the speed of the motion. The observability matrix can be rewritten with constraints as:

$$\mathbf{M}_{\mathbf{S}_k} = \begin{bmatrix} {}^{J}_{I}\mathbf{R}^{I_k}_{I_0}\mathbf{R} & \mathbf{0}_3 & \mathbf{I}_3 & \mathbf{0}_3 & {}^{J}_{I}\mathbf{R}^{I_k}\boldsymbol{\omega}_{I_k} \\ -{}^{G}_{I_k}\mathbf{R}\lfloor {}^{I}\mathbf{p}_J \rfloor {}^{I_k}_{I_0}\mathbf{R} - {}^{G}_{I_0}\mathbf{R}\lfloor {}^{I_0}\mathbf{p}_{I_k} \rfloor & \mathbf{I}_3 & -{}^{G}_{I_k}\mathbf{R}\lfloor {}^{I}\mathbf{p}_J \rfloor {}^{I}_{J}\mathbf{R} & -{}^{G}_{I_k}\mathbf{R}^{I}_{J}\mathbf{R} & {}^{G}\mathbf{v}_{I_k} - {}^{G}_{I_k}\mathbf{R}\lfloor {}^{I}\mathbf{p}_J \rfloor {}^{I_k}\boldsymbol{\omega}_{I_k} \end{bmatrix} \tag{48}$$

$$= \begin{bmatrix} {}^{J}_{I}\mathbf{R}^{I_k}_{I_0}\mathbf{R} & \mathbf{0}_3 & \mathbf{I}_3 & \mathbf{0}_3 & {}^{J}_{I}\mathbf{R}s\mathbf{k} \\ -{}^{G}_{I_k}\mathbf{R}\lfloor {}^{I}\mathbf{p}_J \rfloor {}^{I_k}_{I_0}\mathbf{R} & \mathbf{I}_3 & -{}^{G}_{I_k}\mathbf{R}\lfloor {}^{I}\mathbf{p}_J \rfloor {}^{I}_{J}\mathbf{R} & -{}^{G}_{I_k}\mathbf{R}^{I}_{J}\mathbf{R} & -{}^{G}_{I_k}\mathbf{R}\lfloor {}^{I}\mathbf{p}_J \rfloor {}^{I_0}\boldsymbol{\omega}_{I_0} \end{bmatrix} \tag{49}$$

By applying the above constraint, $\mathbf{N}$ become the null space of $\mathbf{M}_{\mathbf{S}_k}$ (only showing the new directions):

$$\mathbf{M}_{\mathbf{S}_k}\mathbf{N}_3 = \begin{bmatrix} -{}^{J}_{I}\mathbf{R}^{I_k}_{I_0}\mathbf{R}^{I_0}\boldsymbol{\omega}_{I_0} + {}^{J}_{I}\mathbf{R}^{I_k}\boldsymbol{\omega}_{I_k} \\ {}^{G}_{I_k}\mathbf{R}\lfloor {}^{I}\mathbf{p}_J \rfloor {}^{I_k}_{I_0}\mathbf{R}^{I_0}\boldsymbol{\omega}_{I_0} - {}^{G}_{I_k}\mathbf{R}\lfloor {}^{I}\mathbf{p}_J \rfloor {}^{I_k}\boldsymbol{\omega}_{I_k} \end{bmatrix} = \mathbf{0}_{6\times1} \tag{50}$$

This completes the proof. □

Numerical Study: The state estimation with online calibration shows inconsistent estimation results under constant local 1-axis angular velocity motion without translation. Specifically, we have the following values from simulation:

$$\mathbf{k} = \begin{bmatrix} 0 \\ 0 \\ 1 \end{bmatrix}, {}^{J}_{I}\mathbf{R}\mathbf{k} = \begin{bmatrix} 0 \\ 0 \\ 1 \end{bmatrix}, {}^{I_0}\boldsymbol{\omega}_{I_0} = \begin{bmatrix} 0 \\ 0 \\ 0.01 \end{bmatrix} \tag{51}$$

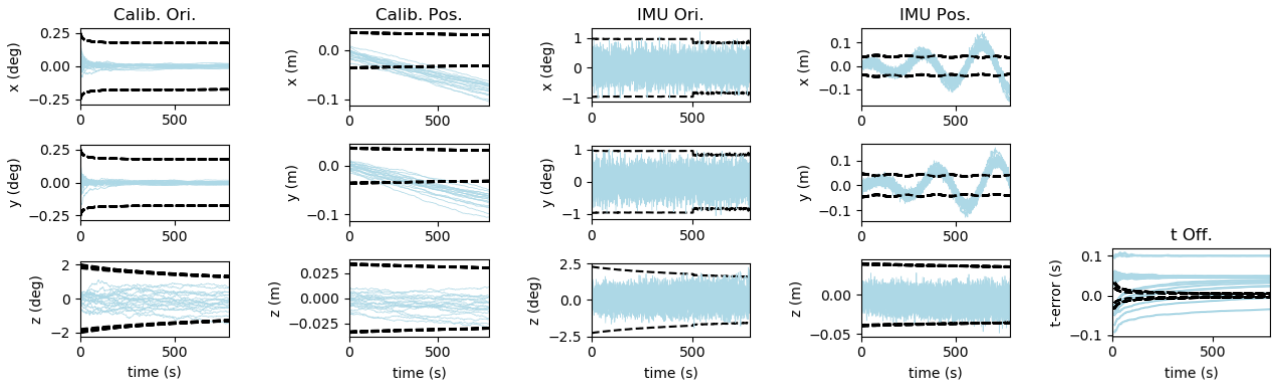

Figure 11: State estimation with online calibration performance across 20 Monte-Carlo simulations where the blue lines are the estimation error and black lines indicate the $\pm3\sigma$ bounds

2.5.8 No Motion

Lemma 2.9. *If the system has no motion, the state is partially unobservable with directions as:*

$$\mathbf{N} = \begin{bmatrix} \mathbf{N}_1 & \mathbf{N}_2 & \mathbf{N}_2 \end{bmatrix} = \begin{bmatrix} \mathbf{I}_3 & \mathbf{0}_3 & \mathbf{0}_{3\times 1} \\ \mathbf{0}_3 & \mathbf{I}_3 & \mathbf{0}_{3\times 1} \\ -{}^{J}_{I}\mathbf{R} & \mathbf{0}_3 & \mathbf{0}_{3\times 1} \\ \mathbf{0}_3 & {}^{J}_{I}\mathbf{R}\,{}^{I_0}_{G}\mathbf{R} & \mathbf{0}_{3\times 1} \\ \mathbf{0}_{1\times 3} & \mathbf{0}_{1\times 3} & 1 \end{bmatrix} \tag{52}$$

The relevant parameters are: ${}^{I_k}_{G}\bar{q},\ {}^{G}\mathbf{p}_{I_k},\ {}^{J}_{I}\bar{q},\ {}^{J}\mathbf{p}_{I},\ {}^{J}t_{I}$.

Proof. The motion constraint can be interpreted as the following geometric constraints:

$${}^{I_0}_{G}\mathbf{R} = {}^{I_k}_{G}\mathbf{R}, \quad {}^{I_k}\boldsymbol{\omega}_{I_k} = {}^{I_0}\boldsymbol{\omega}_{I_0} = \mathbf{0}_{3\times 1}, \quad {}^{I_0}\mathbf{p}_{I_k} = \mathbf{0}_{3\times 1}, \quad {}^{I_k}\mathbf{v}_{I_k} = {}^{I_0}\mathbf{v}_{I_0} = \mathbf{0}_{3\times 1} \tag{53}$$

The observability matrix can be rewritten with constraints as:

$$\mathbf{M}_{\mathbf{S}_k} = \begin{bmatrix} {}^{J}_{I}\mathbf{R}\,{}^{I_k}_{I_0}\mathbf{R} & \mathbf{0}_3 & \mathbf{I}_3 & \mathbf{0}_3 & {}^{J}_{I}\mathbf{R}\,{}^{I_k}\boldsymbol{\omega}_{I_k} \\ -{}^{G}_{I_k}\mathbf{R}\lfloor {}^{I}\mathbf{p}_J \rfloor\, {}^{I_k}_{I_0}\mathbf{R} - {}^{G}_{I_0}\mathbf{R}\lfloor {}^{I_0}\mathbf{p}_{I_k} \rfloor & \mathbf{I}_3 & -{}^{G}_{I_k}\mathbf{R}\lfloor {}^{I}\mathbf{p}_J \rfloor\, {}^{I}_{J}\mathbf{R} & -{}^{G}_{I_k}\mathbf{R}\,{}^{I}_{J}\mathbf{R} & {}^{G}\mathbf{v}_{I_k} - {}^{G}_{I_k}\mathbf{R}\lfloor {}^{I}\mathbf{p}_J \rfloor\, {}^{I_k}\boldsymbol{\omega}_{I_k} \end{bmatrix} \tag{54}$$

$$= \begin{bmatrix} {}^{J}_{I}\mathbf{R} & \mathbf{0}_3 & \mathbf{I}_3 & \mathbf{0}_3 & \mathbf{0}_{3\times 1} \\ -{}^{G}_{I_0}\mathbf{R}\lfloor {}^{I}\mathbf{p}_J \rfloor & \mathbf{I}_3 & -{}^{G}_{I_0}\mathbf{R}\lfloor {}^{I}\mathbf{p}_J \rfloor\, {}^{I}_{J}\mathbf{R} & -{}^{G}_{I_0}\mathbf{R}\,{}^{I}_{J}\mathbf{R} & \mathbf{0}_{3\times 1} \end{bmatrix} \tag{55}$$

By applying the above constraint, $\mathbf{N}$ become the null space of $\mathbf{M}_{\mathbf{S}_k}$:

$$\mathbf{M}_{\mathbf{S}_k}\mathbf{N}_1 = \begin{bmatrix} {}^{J}_{I}\mathbf{R} - {}^{J}_{I}\mathbf{R} \\ -{}^{G}_{I_0}\mathbf{R}\lfloor {}^{I}\mathbf{p}_J \rfloor + {}^{G}_{I_0}\mathbf{R}\lfloor {}^{I}\mathbf{p}_J \rfloor\, {}^{I}_{J}\mathbf{R}\,{}^{J}_{I}\mathbf{R} \end{bmatrix} = \mathbf{0}_{6\times 3} \tag{56}$$

$$\mathbf{M}_{\mathbf{S}_k}\mathbf{N}_2 = \begin{bmatrix} \mathbf{0}_3 \\ \mathbf{I}_3 - {}^{G}_{I_0}\mathbf{R}\,{}^{I}_{J}\mathbf{R}\,{}^{J}_{I}\mathbf{R}\,{}^{I_0}_{G}\mathbf{R} \end{bmatrix} = \mathbf{0}_{6\times 3} \tag{57}$$

$$\mathbf{M}_{\mathbf{S}_k}\mathbf{N}_3 = \mathbf{0}_{6\times 1} \tag{58}$$

This completes the proof. □

Numerical Study: The state estimation with online calibration shows inconsistent estimation results under no motion. Specifically, we have the following values from simulation:

$${}^{J}_{I}\mathbf{R} = \begin{bmatrix} 1 & 0 & 0 \\ 0 & 1 & 0 \\ 0 & 0 & 1 \end{bmatrix}, {}^{J}_{I}\mathbf{R}\,{}^{I_0}_{G}\mathbf{R} = \begin{bmatrix} 1 & 0 & 0 \\ 0 & 1 & 0 \\ 0 & 0 & 1 \end{bmatrix} \tag{59}$$

which makes the z-axis of position estimation of both calibration and robot pose partially unobservable.

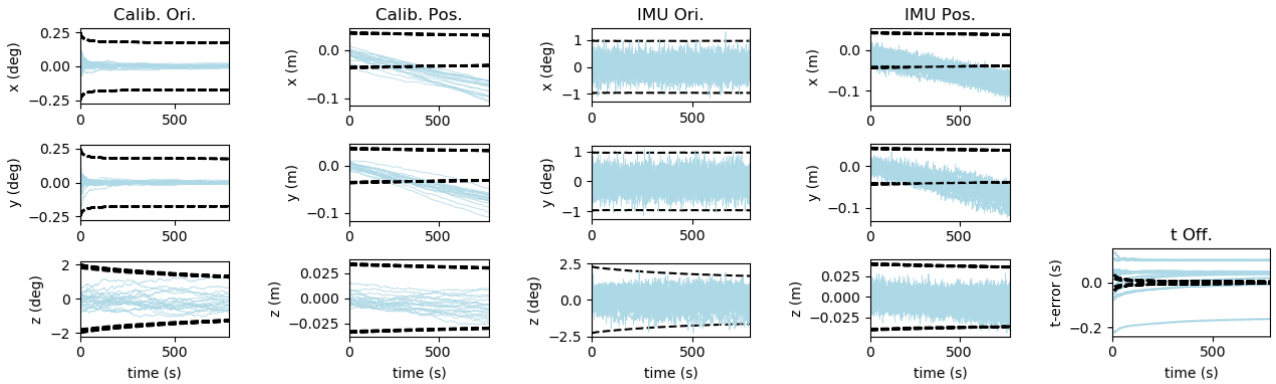

Figure 12: State estimation with online calibration performance across 20 Monte-Carlo simulations where the blue lines are the estimation error and black lines indicate the $\pm 3\sigma$ bounds

3 Degenerate Motions: Asynchronous Global and Local Sensor Pair

In analogy to synchronous sensor pair analysis, in this section, we present degenerate motion analysis of the asynchronous global and local sensor pair, leveraging the linear pose interpolation method [6] to handle the synchronicity. Note we omit numerical study in this section as they show very similar results to the previous section.

3.1 State to Analyze

In analogy to the state for synchronous measurement (see Eq. (1)), we have the following state vector at t_k:

$$\mathbf{x}_{\mathbf{A}_k} = \begin{bmatrix} {}^{I_k}_{G}\bar{q}^\top & {}^{G}\mathbf{p}_{I_k}^\top & {}^{I_{k-1}}_{G}\bar{q}^\top & {}^{G}\mathbf{p}_{I_{k-1}}^\top & {}^{J}_{I}\bar{q}^\top & {}^{J}\mathbf{p}_{I}^\top & {}^{J}t_I \end{bmatrix}^\top \tag{60}$$

Note that the state now has an additional sensor $\{I\}$ pose at $t_{k-1}({}^{I_{k-1}}_{G}\bar{q}, {}^{G}\mathbf{p}_{I_{k-1}})$ to handle asynchronous measurement. The corresponding error state is now can be shown as:

$$\tilde{\mathbf{x}}_{\mathbf{A}_k} = \begin{bmatrix} {}^{I_k}_{G}\tilde{\boldsymbol{\theta}}^\top & {}^{G}\tilde{\mathbf{p}}_{I_k}^\top & {}^{I_{k-1}}_{G}\tilde{\boldsymbol{\theta}}^\top & {}^{G}\tilde{\mathbf{p}}_{I_{k-1}}^\top & {}^{J}_{I}\tilde{\boldsymbol{\theta}}^\top & {}^{J}\tilde{\mathbf{p}}_{I}^\top & {}^{J}\tilde{t}_I \end{bmatrix}^\top \tag{61}$$

3.2 State Propagation model with Local Sensor $\{I\}$

At time t_k, we leverage the local sensor's current relative pose information $\{{}^{I_k}_{I_{k-1}}\bar{q}, {}^{I_{k-1}}\mathbf{p}_{I_k}\}$ and previous relative pose information $\{{}^{I_{k-1}}_{I_{k-2}}\bar{q}, {}^{I_{k-2}}\mathbf{p}_{I_{k-1}}\}$, to propagate two poses in the state, Eq. (60), from t_{k-1} to t_k as:

$${}^{I_k}_{G}\bar{q} = {}^{I_k}_{I_{k-1}}\bar{q} \boxplus {}^{I_{k-1}}_{G}\bar{q}, \quad {}^{G}\mathbf{p}_{I_k} = {}^{G}\mathbf{p}_{I_{k-1}} + {}^{G}_{I_{k-1}}\mathbf{R}\,{}^{I_{k-1}}\mathbf{p}_{I_k} \tag{62}$$

$${}^{I_{k-1}}_{G}\bar{q} = {}^{I_{k-1}}_{I_{k-2}}\bar{q} \boxplus {}^{I_{k-2}}_{G}\bar{q}, \quad {}^{G}\mathbf{p}_{I_{k-1}} = {}^{G}\mathbf{p}_{I_{k-2}} + {}^{G}_{I_{k-2}}\mathbf{R}\,{}^{I_{k-2}}\mathbf{p}_{I_{k-1}} \tag{63}$$

while the calibration states remain the same. The corresponding error state transition can be shown as:

$$\boldsymbol{\Phi}(t_k, t_{k-1}) = \begin{bmatrix} {}^{I_k}_{I_{k-1}}\mathbf{R} & \mathbf{0}_3 & \mathbf{0}_3 & \mathbf{0}_3 & \mathbf{0}_3 & \mathbf{0}_3 & \mathbf{0}_{3\times1} \\ -{}^{G}_{I_{k-1}}\mathbf{R}\lfloor {}^{I_{k-1}}\mathbf{p}_{I_k} \rfloor & \mathbf{I}_3 & \mathbf{0}_3 & \mathbf{0}_3 & \mathbf{0}_3 & \mathbf{0}_3 & \mathbf{0}_{3\times1} \\ \mathbf{0}_3 & \mathbf{0}_3 & {}^{I_{k-1}}_{I_{k-2}}\mathbf{R} & \mathbf{0}_3 & \mathbf{0}_3 & \mathbf{0}_3 & \mathbf{0}_{3\times1} \\ \mathbf{0}_3 & \mathbf{0}_3 & -{}^{G}_{I_{k-2}}\mathbf{R}\lfloor {}^{I_{k-2}}\mathbf{p}_{I_{k-1}} \rfloor & \mathbf{I}_3 & \mathbf{0}_3 & \mathbf{0}_3 & \mathbf{0}_{3\times1} \\ \mathbf{0}_3 & \mathbf{0}_3 & \mathbf{0}_3 & \mathbf{0}_3 & \mathbf{I}_3 & \mathbf{0}_3 & \mathbf{0}_{3\times1} \\ \mathbf{0}_3 & \mathbf{0}_3 & \mathbf{0}_3 & \mathbf{0}_3 & \mathbf{0}_3 & \mathbf{I}_3 & \mathbf{0}_{3\times1} \\ \mathbf{0}_{1\times3} & \mathbf{0}_{1\times3} & \mathbf{0}_{1\times3} & \mathbf{0}_{1\times3} & \mathbf{0}_{1\times3} & \mathbf{0}_{1\times3} & 1 \end{bmatrix} \tag{64}$$

3.3 State Update model with Global Sensor $\{J\}$

Assume we have a pose measurement of sensor $\{J\}$ at time t'_k, where $t_{k-1} \leq t'_k + {}^{J}t_I \leq t_k$. Note that t_{k-1} and t_k are the timestamps of sensor $\{I\}$ pose in the state. The measurement can be modeled as follows:

$$\mathbf{z}_{\mathbf{A}_k} := \begin{bmatrix} {}^{J_{k'}}_{G}\boldsymbol{\theta} \\ {}^{G}\mathbf{p}_{J_{k'}} \end{bmatrix} = \begin{bmatrix} \mathrm{Log}({}^{J}_{I}\mathbf{R}\,{}^{I_{k'}}_{G}\mathbf{R}) \\ {}^{G}\mathbf{p}_{I_k} + {}^{G}_{I_{k'}}\mathbf{R}\,{}^{I}\mathbf{p}_{J} \end{bmatrix} := \mathbf{h}(\mathbf{x}_{\mathbf{A}_k}) \tag{65}$$

Due to asynchronicity of the measurement, the exact pose $\{{}^{I_{k'}}_{G}\mathbf{R}, {}^{G}\mathbf{p}_{I_{k'}}\}$ does not exist in the state vector. The pose can be approximated by using linear interpolation of two bounding poses [6]:

$${}^{G}_{I_{k'}}\mathbf{R} = {}^{G}_{I_{k-1}}\mathbf{R}\mathrm{Exp}(\lambda\ \mathrm{Log}({}^{I_{k-1}}_{G}\mathbf{R}\,{}^{G}_{I_k}\mathbf{R})) \tag{66}$$

$${}^{G}\mathbf{p}_{I_{k'}} = (1-\lambda)\,{}^{G}\mathbf{p}_{I_{k-1}} + \lambda\,{}^{G}\mathbf{p}_{I_k} \tag{67}$$

$$\lambda = \frac{t'_k + {}^{J}t_I - t_{k-1}}{t_k - t_{k-1}} \tag{68}$$

where $\text{Exp}(\cdot)$ is the SO(3) matrix exponential functions [4]. The measurement model can be linearized at the state estimate $\hat{\mathbf{x}}_{\mathbf{A}_k}$ as:

$$\tilde{\mathbf{z}}_{\mathbf{A}_k} := \mathbf{z}_{\mathbf{A}_k} - \mathbf{h}(\hat{\mathbf{x}}_{\mathbf{A}_k}) = \mathbf{H}_{\mathbf{A}_k}\tilde{\mathbf{x}}_{\mathbf{A}_k} \tag{69}$$

where $\mathbf{H}_{\mathbf{A}_k}$ is the Jacobian matrix:

$$\mathbf{H}_{\mathbf{A}_k} = \begin{bmatrix} \frac{\partial {}^{J_k}_{G}\boldsymbol{\theta}}{\partial {}^{I_k}_{G}\boldsymbol{\theta}} & \frac{\partial {}^{J_k}_{G}\boldsymbol{\theta}}{\partial {}^{G}\mathbf{p}_{I_k}} & \frac{\partial {}^{J_k}_{G}\boldsymbol{\theta}}{\partial {}^{I_{k-1}}_{G}\boldsymbol{\theta}} & \frac{\partial {}^{J_k}_{G}\boldsymbol{\theta}}{\partial {}^{G}\mathbf{p}_{I_{k-1}}} & \frac{\partial {}^{J_k}_{G}\boldsymbol{\theta}}{\partial {}^{J}_{I}\boldsymbol{\theta}} & \frac{\partial {}^{J_k}_{G}\boldsymbol{\theta}}{\partial {}^{J}\mathbf{p}_{I}} & \frac{\partial {}^{J_k}_{G}\boldsymbol{\theta}}{\partial {}^{J}t_{I}} \\ \frac{\partial {}^{G}\mathbf{p}_{J_k}}{\partial {}^{I_k}_{G}\boldsymbol{\theta}} & \frac{\partial {}^{G}\mathbf{p}_{J_k}}{\partial {}^{G}\mathbf{p}_{I_k}} & \frac{\partial {}^{G}\mathbf{p}_{J_k}}{\partial {}^{I_{k-1}}_{G}\boldsymbol{\theta}} & \frac{\partial {}^{G}\mathbf{p}_{J_k}}{\partial {}^{G}\mathbf{p}_{I_{k-1}}} & \frac{\partial {}^{G}\mathbf{p}_{J_k}}{\partial {}^{J}_{I}\boldsymbol{\theta}} & \frac{\partial {}^{G}\mathbf{p}_{J_k}}{\partial {}^{J}\mathbf{p}_{I}} & \frac{\partial {}^{G}\mathbf{p}_{J_k}}{\partial {}^{J}t_{I}} \end{bmatrix} \tag{70}$$

$$= \begin{bmatrix} {}^{J}_{I}\mathbf{R}\boldsymbol{\Upsilon}_1 & \mathbf{0}_3 & {}^{J}_{I}\mathbf{R}\boldsymbol{\Upsilon}_2 & \mathbf{0}_3 & \mathbf{I}_3 & \mathbf{0}_3 & {}^{J}_{I}\mathbf{R}\boldsymbol{\Upsilon}_3 \\ -{}^{G}_{I_{k'}}\mathbf{R}\lfloor {}^{I}\mathbf{p}_J \rfloor \boldsymbol{\Upsilon}_1 & \lambda\mathbf{I}_3 & -{}^{G}_{I_{k'}}\mathbf{R}\lfloor {}^{I}\mathbf{p}_J \rfloor \boldsymbol{\Upsilon}_2 & (1-\lambda)\mathbf{I}_3 & -{}^{G}_{I_{k'}}\mathbf{R}\lfloor {}^{I}\mathbf{p}_J \rfloor {}^{I}_{J}\mathbf{R} & -{}^{G}_{I_{k'}}\mathbf{R}{}^{I}_{J}\mathbf{R} & \boldsymbol{\Upsilon}_4 - {}^{G}_{I_{k'}}\mathbf{R}\lfloor {}^{I}\mathbf{p}_J \rfloor \boldsymbol{\Upsilon}_3 \end{bmatrix} \tag{71}$$

where

$$\boldsymbol{\Upsilon}_1 = \lambda \mathbf{J}_\mathbf{r}(\lambda {}^{I_{k-1}}_{I_k}\boldsymbol{\theta})\mathbf{J}_\mathbf{r}^{-1}({}^{I_{k-1}}_{I_k}\boldsymbol{\theta}) \qquad \boldsymbol{\Upsilon}_2 = \mathbf{J}_\mathbf{r}(\lambda {}^{I_{k-1}}_{I_k}\boldsymbol{\theta})(\mathbf{J}_\mathbf{l}^{-1}(\lambda {}^{I_{k-1}}_{I_k}\boldsymbol{\theta}) - \lambda \mathbf{J}_\mathbf{l}^{-1}({}^{I_{k-1}}_{I_k}\boldsymbol{\theta})) \tag{72}$$

$$\boldsymbol{\Upsilon}_3 = \frac{1}{t_k - t_{k-1}} {}^{I_{k-1}}_{I_k}\boldsymbol{\theta} \qquad \boldsymbol{\Upsilon}_4 = \frac{1}{t_k - t_{k-1}}({}^{G}\mathbf{p}_{I_k} - {}^{G}\mathbf{p}_{I_{k-1}}) \tag{73}$$

3.4 Observability Matrix

In analogy to the observability matrix (Eq. (12)), we have the following row of the observability matrix of asynchronous measurement case:

$$\mathbf{M}_{\mathbf{A}_k} := \mathbf{M}_{\mathbf{A}_k}\boldsymbol{\Phi}_\mathbf{A}(t_k, t_0) \tag{74}$$

$$= \begin{bmatrix} {}^{J}_{I}\mathbf{R}\boldsymbol{\Upsilon}_1 {}^{I_k}_{I_0}\mathbf{R} & \mathbf{0}_3 & {}^{J}_{I}\mathbf{R}\boldsymbol{\Upsilon}_2 {}^{I_{k-1}}_{I_0}\mathbf{R} & \mathbf{0}_3 & \mathbf{I}_3 & \mathbf{0}_3 & {}^{J}_{I}\mathbf{R}\boldsymbol{\Upsilon}_3 \\ -{}^{G}_{I_{k'}}\mathbf{R}\lfloor {}^{I}\mathbf{p}_J \rfloor \boldsymbol{\Upsilon}_1 {}^{I_k}_{I_0}\mathbf{R} - \lambda {}^{G}_{I_0}\mathbf{R}\lfloor {}^{I_0}\mathbf{p}_{I_k} \rfloor & \lambda\mathbf{I}_3 & -{}^{G}_{I_{k'}}\mathbf{R}\lfloor {}^{I}\mathbf{p}_J \rfloor \boldsymbol{\Upsilon}_2 {}^{I_{k-1}}_{I_0}\mathbf{R} - (1-\lambda){}^{G}_{I_0}\mathbf{R}\lfloor {}^{I_0}\mathbf{p}_{I_{k-1}} \rfloor & (1-\lambda)\mathbf{I}_3 & -{}^{G}_{I_{k'}}\mathbf{R}\lfloor {}^{I}\mathbf{p}_J \rfloor {}^{I}_{J}\mathbf{R} & -{}^{G}_{I_{k'}}\mathbf{R}{}^{I}_{J}\mathbf{R} & \boldsymbol{\Upsilon}_4 - {}^{G}_{I_{k'}}\mathbf{R}\lfloor {}^{I}\mathbf{p}_J \rfloor \boldsymbol{\Upsilon}_3 \end{bmatrix} \tag{75}$$

3.4.1 General Motion

Lemma 3.1. *If the system undergoes general 3D motion with fully exited more than 1 axis rotation, the state is fully observable [7, 8].*

3.5 Degenerate Motion Analysis

By analyzing the observability matrix $\mathbf{M}_{\mathbf{A}_k}$, we identify the following degenerate motions that cause the state to be partially unobservable.

3.5.1 1-Axis Rotation and General 3-Axis Translation Motion

Lemma 3.2. *If the system undergoes 1-axis rotation and general 3-axis translation motion, the state is partially unobservable with directions as:*

$$\mathbf{N} = \begin{bmatrix} \mathbf{0}_{3\times1} \\ \mathbf{k} \\ \mathbf{0}_{3\times1} \\ \mathbf{k} \\ \mathbf{0}_{3\times1} \\ {}^{J}_{I}\mathbf{R}\mathbf{k} \\ 0 \end{bmatrix} \tag{76}$$

where $\mathbf{k}$ *is the rotation axis. The relevant parameters are:* ${}^{G}\mathbf{p}_{I_k}, {}^{G}\mathbf{p}_{I_{k-1}}, {}^{J}\mathbf{p}_{I}$.

Proof. The motion constraint can be interpreted as the following geometric constraints:

$${}^{I_0}_{G}\mathbf{R}\mathbf{k} = {}^{I_k}_{G}\mathbf{R}\mathbf{k} = {}^{I_{k'}}_{G}\mathbf{R}\mathbf{k} = \mathbf{k} \tag{77}$$

We can find $\mathbf{N}$ is the null space of $\mathbf{M}_{\mathbf{A}_k}$ with the above constraints:

$$\mathbf{M}_{\mathbf{A}_k}\mathbf{N} = \begin{bmatrix} \mathbf{0}_{3\times1} \\ \lambda\mathbf{k} + (1-\lambda)\mathbf{k} - {}^{G}_{I_{k'}}\mathbf{R}^{I}_{J}\mathbf{R}^{J}_{I}\mathbf{R}\mathbf{k} \end{bmatrix} = \mathbf{0}_{6\times1} \tag{78}$$

This completes the proof. □

3.5.2 Constant Local Angular and Linear Velocity Motion

Lemma 3.3. *If the system undergoes constant local angular and linear velocity motion, the state is partially unobservable with directions as:*

$$\mathbf{N} = \begin{bmatrix} \mathbf{N}_1 & \mathbf{N}_2 \end{bmatrix} = \begin{bmatrix} \mathbf{0}_{3\times1} & \mathbf{0}_{3\times1} \\ \mathbf{k} & \mathbf{0}_{3\times1} \\ \mathbf{0}_{3\times1} & \mathbf{0}_{3\times1} \\ \mathbf{k} & \mathbf{0}_{3\times1} \\ \mathbf{0}_{3\times1} & -{}^{J}_{I}\mathbf{R}^{I_0}\boldsymbol{\omega}_{I_0} \\ {}^{J}_{I}\mathbf{R}\mathbf{k} & {}^{J}_{I}\mathbf{R}^{I_0}\mathbf{v}_{I_0} \\ 0 & 1 \end{bmatrix} \tag{79}$$

where $\mathbf{k}$ *is the angular velocity axis of rotation. The relevant parameters are:* ${}^{G}\mathbf{p}_{I_k}, {}^{G}\mathbf{p}_{I_{k-1}}, {}^{J}_{I}\bar{q}, {}^{J}\mathbf{p}_{I}, {}^{J}t_{I}$.

Proof. The motion constraint can be interpreted as the following geometric constraints:

$${}^{I_0}_{G}\mathbf{R}\mathbf{k} = {}^{I_k}_{G}\mathbf{R}\mathbf{k} = {}^{I_{k'}}_{G}\mathbf{R}\mathbf{k} = \mathbf{k}, \quad \boldsymbol{\Upsilon}_3 = \frac{{}^{I_{k-1}}_{I_k}\boldsymbol{\theta}}{t_k - t_{k-1}} = \frac{{}^{I_{k-1}}\boldsymbol{\omega}_{I_{k-1}}(t_k - t_{k-1})}{t_k - t_{k-1}} = {}^{I_k}\boldsymbol{\omega}_{I_k} = {}^{I_0}\boldsymbol{\omega}_{I_0} \tag{80}$$

$$\boldsymbol{\Upsilon}_4 = \frac{{}^{G}\mathbf{p}_{I_k} - {}^{G}\mathbf{p}_{I_{k-1}}}{t_k - t_{k-1}} = \frac{{}^{G}\mathbf{v}_{I_0}t_k - {}^{G}\mathbf{v}_{I_0}t_{k-1}}{t_k - t_{k-1}} = {}^{G}\mathbf{v}_{I_k} = {}^{G}\mathbf{v}_{I_0} \tag{81}$$

By applying the above constraints, $\mathbf{N}$ become the null space of $\mathbf{M}_{\mathbf{A}_k}$ (only showing the new directions):

$$\mathbf{M}_{\mathbf{A}_k}\mathbf{N}_2 = \begin{bmatrix} -{}^{J}_{I}\mathbf{R}^{I_0}\boldsymbol{\omega}_{I_0} + {}^{J}_{I}\mathbf{R}\boldsymbol{\Upsilon}_3 \\ {}^{G}_{I_{k'}}\mathbf{R}\lfloor {}^{I}\mathbf{p}_{J} \rfloor {}^{I}_{J}\mathbf{R}^{J}_{I}\mathbf{R}^{I_0}\boldsymbol{\omega}_{I_0} - {}^{G}_{I_{k'}}\mathbf{R}^{I}_{J}\mathbf{R}^{J}_{I}\mathbf{R}^{I_0}\mathbf{v}_{I_0} + \boldsymbol{\Upsilon}_4 - {}^{G}_{I_{k'}}\mathbf{R}\lfloor {}^{I}\mathbf{p}_{J} \rfloor \boldsymbol{\Upsilon}_3 \end{bmatrix} = \mathbf{0}_{6\times1} \tag{82}$$

This completes the proof. □

3.5.3 3-Axis or 2-Axis Translation without Rotation Motion

Lemma 3.4. *If the system undergoes pure 3D translation or 2D translation (planar) motion, the state is partially unobservable with directions as:*

$$\mathbf{N} = \begin{bmatrix} \mathbf{0}_3 \\ \mathbf{I} \\ \mathbf{0}_3 \\ \mathbf{I} \\ \mathbf{0}_3 \\ {}^{J}_{I}\mathbf{R}\,{}^{I_0}_{G}\mathbf{R} \\ \mathbf{0}_{1\times 3} \end{bmatrix} \tag{83}$$

The relevant parameters are: ${}^{G}\mathbf{p}_{I_k}, {}^{G}\mathbf{p}_{I_{k-1}}, \ {}^{J}\mathbf{p}_{I}$.

Proof. The motion constraint can be interpreted as the following geometric constraints:

$${}^{I_0}_{G}\mathbf{R} = {}^{I_k}_{G}\mathbf{R} = {}^{I_{k'}}_{G}\mathbf{R}, \quad {}^{I_k}\boldsymbol{\omega}_{I_k} = {}^{I_0}\boldsymbol{\omega}_{I_0} = \mathbf{0}_{3\times 1} \tag{84}$$

By applying the above constraints, $\mathbf{N}$ become the null space of $\mathbf{M}_{\mathbf{A}_k}$:

$$\mathbf{M}_{\mathbf{A}_k}\mathbf{N} = \begin{bmatrix} \mathbf{0}_3 \\ \lambda\mathbf{I}_3 + (1-\lambda)\mathbf{I}_3 - {}^{G}_{I_{k'}}\mathbf{R}\,{}^{I}_{J}\mathbf{R}\,{}^{J}_{I}\mathbf{R}\,{}^{I_0}_{G}\mathbf{R} \end{bmatrix} = \mathbf{0}_{6\times 1} \tag{85}$$

This completes the proof. □

3.5.4 1-Axis Translation without Rotation Motion

Lemma 3.5. *If the system undergoes general local 1-axis translation (straight line motion with general velocity) without rotation, the state is partially unobservable with directions as:*

$$\mathbf{N} = \begin{bmatrix} \mathbf{N}_1 & \mathbf{N}_2 \end{bmatrix} = \begin{bmatrix} \mathbf{k} & \mathbf{0}_3 \\ \mathbf{0}_{3\times 1} & \mathbf{I}_3 \\ \mathbf{k} & \mathbf{0}_3 \\ \mathbf{0}_{3\times 1} & \mathbf{I}_3 \\ -{}^{J}_{I}\mathbf{R}\mathbf{k} & \mathbf{0}_3 \\ \mathbf{0}_{3\times 1} & {}^{J}_{I}\mathbf{R}\,{}^{I_0}_{G}\mathbf{R} \\ 0 & \mathbf{0}_{1\times 3} \end{bmatrix} \tag{86}$$

where $\mathbf{k}$ *is the axis of the translation. The relevant parameters are:* ${}^{I_k}_{G}\bar{q}, \ {}^{G}\mathbf{p}_{I_k}, {}^{I_{k-1}}_{G}\bar{q}, \ {}^{G}\mathbf{p}_{I_{k-1}}, \ {}^{J}_{I}\bar{q}, \ {}^{J}\mathbf{p}_{I}$.

Proof. The motion constraint can be interpreted as the following geometric constraints:

$${}^{I_0}_{G}\mathbf{R} = {}^{I_k}_{G}\mathbf{R}, \quad {}^{I_k}\boldsymbol{\omega}_{I_k} = {}^{I_0}\boldsymbol{\omega}_{I_0} = \mathbf{0}_{3\times 1}, \quad {}^{I_0}\mathbf{p}_{I_k} = f(t_k)\mathbf{k}, \quad {}^{I_0}\mathbf{p}_{I_{k-1}} = f(t_{k-1})\mathbf{k} \tag{87}$$

$$\boldsymbol{\Upsilon}_1 = \lambda\mathbf{I}_3, \quad \boldsymbol{\Upsilon}_2 = (1-\lambda)\mathbf{I}_3, \quad \boldsymbol{\Upsilon}_3 = \mathbf{0}_{3\times 1} \tag{88}$$

where $f(\cdot)$ is a scalar function.

By applying the above constraint, $\mathbf{N}$ become the null space of $\mathbf{M}_{\mathbf{A}_k}$:

$$\begin{aligned} \mathbf{M}_{\mathbf{A}_k}\mathbf{N}_1 &= \begin{bmatrix} {}^{J}_{I}\mathbf{R}\boldsymbol{\Upsilon}_1\,{}^{I_k}_{I_0}\mathbf{R}\mathbf{k} + {}^{J}_{I}\mathbf{R}\boldsymbol{\Upsilon}_2\,{}^{I_{k-1}}_{I_0}\mathbf{R}\mathbf{k} - {}^{J}_{I}\mathbf{R}\mathbf{k} \\ -{}^{G}_{I_{k'}}\mathbf{R}\lfloor {}^{I}\mathbf{p}_J \rfloor \boldsymbol{\Upsilon}_1\,{}^{I_k}_{I_0}\mathbf{R}\mathbf{k} - \lambda\,{}^{G}_{I_0}\mathbf{R}\lfloor {}^{I_0}\mathbf{p}_{I_k} \rfloor \mathbf{k} - {}^{G}_{I_{k'}}\mathbf{R}\lfloor {}^{I}\mathbf{p}_J \rfloor \boldsymbol{\Upsilon}_2\,{}^{I_{k-1}}_{I_0}\mathbf{R}\mathbf{k} - (1-\lambda)\,{}^{G}_{I_0}\mathbf{R}\lfloor {}^{I_0}\mathbf{p}_{I_{k-1}} \rfloor \mathbf{k} + {}^{G}_{I_{k'}}\mathbf{R}\lfloor {}^{I}\mathbf{p}_J \rfloor\, {}^{J}_{I}\mathbf{R}\,{}^{J}_{I}\mathbf{R}\mathbf{k} \end{bmatrix} \\ &= \begin{bmatrix} \mathbf{0}_{3\times 1} \\ -{}^{G}_{I_{k'}}\mathbf{R}\lfloor {}^{I}\mathbf{p}_J \rfloor \mathbf{k} - \lambda\,{}^{G}_{I_0}\mathbf{R}\lfloor f(t_k)\mathbf{k} \rfloor \mathbf{k} - (1-\lambda)\,{}^{G}_{I_0}\mathbf{R}\lfloor f(t_{k-1})\mathbf{k} \rfloor \mathbf{k} + {}^{G}_{I_{k'}}\mathbf{R}\lfloor {}^{I}\mathbf{p}_J \rfloor \mathbf{k} \end{bmatrix} = \mathbf{0}_{6\times 1} \end{aligned} \tag{89}$$

$$\mathbf{M}_{\mathbf{A}_k}\mathbf{N}_2 = \begin{bmatrix} \mathbf{0}_3 \\ \lambda\mathbf{I}_3 + (1-\lambda)\mathbf{I}_3 - {}^{G}_{I_{k'}}\mathbf{R}\,{}^{I}_{J}\mathbf{R}\,{}^{J}_{I}\mathbf{R}\,{}^{I_0}_{G}\mathbf{R} \end{bmatrix} = \mathbf{0}_{6\times 3} \tag{90}$$

This completes the proof. □

3.5.5 Constant Velocity 1-Axis Translation without Rotation Motion

Lemma 3.6. *If the system undergoes constant local linear velocity motion (straight line motion with constant velocity) without rotation, the state is partially unobservable with directions as:*

$$\mathbf{N} = \begin{bmatrix} \mathbf{N}_1 & \mathbf{N}_2 & \mathbf{N}_3 \end{bmatrix} = \begin{bmatrix} \mathbf{k} & \mathbf{0}_3 & \mathbf{0}_{3\times 1} \\ \mathbf{0}_{3\times 1} & \mathbf{I}_3 & -{}^G\mathbf{v}_{I_0} \\ \mathbf{k} & \mathbf{0}_3 & \mathbf{0}_{3\times 1} \\ \mathbf{0}_{3\times 1} & \mathbf{I}_3 & -{}^G\mathbf{v}_{I_0} \\ -{}^J_I\mathbf{R}\mathbf{k} & \mathbf{0}_3 & \mathbf{0}_{3\times 1} \\ \mathbf{0}_{3\times 1} & {}^J_I\mathbf{R}\,{}^{I_0}_G\mathbf{R} & \mathbf{0}_{3\times 1} \\ 0 & \mathbf{0}_{1\times 3} & 1 \end{bmatrix} \tag{91}$$

where $\mathbf{k}$ *is the axis of the translation. The relevant parameters are:* ${}^{I_k}_G\bar{q},\ {}^G\mathbf{p}_{I_k}, {}^{I_{k-1}}_G\bar{q},\ {}^G\mathbf{p}_{I_{k-1}},\ {}^J_I\bar{q},\ {}^J\mathbf{p}_I,\ {}^Jt_I$.

Proof. The motion constraint can be interpreted as the following geometric constraints:

$${}^{I_0}_G\mathbf{R} = {}^{I_k}_G\mathbf{R}, \quad {}^{I_k}\boldsymbol{\omega}_{I_k} = {}^{I_0}\boldsymbol{\omega}_{I_0} = \mathbf{0}_{3\times 1}, \quad {}^{I_0}\mathbf{p}_{I_k} = f(t_k)\mathbf{k}, \quad {}^{I_0}\mathbf{p}_{I_{k-1}} = f(t_{k-1})\mathbf{k}, \boldsymbol{\Upsilon}_1 = \lambda\mathbf{I}_3 \tag{92}$$

$$\boldsymbol{\Upsilon}_2 = (1-\lambda)\mathbf{I}_3, \quad \boldsymbol{\Upsilon}_3 = \mathbf{0}_{3\times 1}, \boldsymbol{\Upsilon}_4 = \frac{{}^G\mathbf{p}_{I_k} - {}^G\mathbf{p}_{I_{k-1}}}{t_k - t_{k-1}} = \frac{{}^G\mathbf{v}_{I_0}t_k - {}^G\mathbf{v}_{I_0}t_{k-1}}{t_k - t_{k-1}} = {}^G\mathbf{v}_{I_k} = {}^G\mathbf{v}_{I_0} \tag{93}$$

where $f(\cdot)$ is a scalar function and s is the speed of the motion. By applying the above constraint, $\mathbf{N}$ become the null space of $\mathbf{M}_{\mathbf{A}_k}$ (only showing the new directions):

$$\mathbf{M}_{\mathbf{A}_k}\mathbf{N}_3 = \begin{bmatrix} \mathbf{0}_{3\times 1} \\ -\lambda{}^G\mathbf{v}_{I_0} - (1-\lambda){}^G\mathbf{v}_{I_0} + \boldsymbol{\Upsilon}_4 \end{bmatrix} = \mathbf{0}_{6\times 1} \tag{94}$$

This completes the proof. □

3.5.6 1-Axis Rotation without Translation Motion

Lemma 3.7. *If the system undergoes general local 1-axis rotation without translation, the state is partially unobservable with directions as:*

$$\mathbf{N} = \begin{bmatrix} \mathbf{N}_1 & \mathbf{N}_2 \end{bmatrix} = \begin{bmatrix} \mathbf{k} & \mathbf{0}_{3\times 1} \\ \mathbf{0}_{3\times 1} & \mathbf{k} \\ \mathbf{k} & \mathbf{0}_{3\times 1} \\ \mathbf{0}_{3\times 1} & \mathbf{k} \\ -{}^J_I\mathbf{R}\mathbf{k} & \mathbf{0}_{3\times 1} \\ \mathbf{0}_{3\times 1} & {}^J_I\mathbf{R}\mathbf{k} \\ 0 & 0 \end{bmatrix} \tag{95}$$

where $\mathbf{k}$ *is the rotation axis. The relevant parameters are:* ${}^{I_k}_G\bar{q},\ {}^G\mathbf{p}_{I_k}, {}^{I_{k-1}}_G\bar{q},\ {}^G\mathbf{p}_{I_{k-1}},\ {}^J_I\bar{q},\ {}^J\mathbf{p}_I$.

Proof. The motion constraint can be interpreted as the following geometric constraints:

$${}^{I_0}_G\mathbf{R}\mathbf{k} = {}^{I_k}_G\mathbf{R}\mathbf{k} = \mathbf{k}, \quad {}^{I_0}\mathbf{p}_{I_k} = \mathbf{0}_{3\times 1}, \quad {}^{I_k}\mathbf{v}_{I_k} = {}^{I_0}\mathbf{v}_{I_0} = \mathbf{0}_{3\times 1} \tag{96}$$

$$\boldsymbol{\Upsilon}_1\mathbf{k} = \lambda\mathbf{J}_\mathbf{r}(\lambda^{I_{k-1}}_{I_k}\boldsymbol{\theta})\mathbf{J}_\mathbf{r}^{-1}({}^{I_{k-1}}_{I_k}\boldsymbol{\theta})\mathbf{k} = \lambda\mathbf{k}, \quad \boldsymbol{\Upsilon}_2\mathbf{k} = \mathbf{J}_\mathbf{r}(\lambda^{I_{k-1}}_{I_k}\boldsymbol{\theta})(\mathbf{J}_\mathbf{l}^{-1}(\lambda^{I_{k-1}}_{I_k}\boldsymbol{\theta}) - \lambda\mathbf{J}_\mathbf{l}^{-1}({}^{I_{k-1}}_{I_k}\boldsymbol{\theta}))\mathbf{k} = (1-\lambda)\mathbf{k}$$

By applying the above constraint, $\mathbf{N}$ become the null space of $\mathbf{M}_{\mathbf{A}_k}$:

$$\mathbf{M}_{\mathbf{A}_k}\mathbf{N}_1 = \begin{bmatrix} {}^J_I\mathbf{R}\boldsymbol{\Upsilon}_1{}^{I_k}_{I_0}\mathbf{R}\mathbf{k} + {}^J_I\mathbf{R}\boldsymbol{\Upsilon}_2{}^{I_{k-1}}_{I_0}\mathbf{R}\mathbf{k} - {}^J_I\mathbf{R}\mathbf{k} \\ -{}^G_{I_{k'}}\mathbf{R}\lfloor{}^I\mathbf{p}_J\rfloor\boldsymbol{\Upsilon}_1{}^{I_k}_{I_0}\mathbf{R}\mathbf{k} - \lambda{}^G_{I_0}\mathbf{R}\lfloor{}^{I_0}\mathbf{p}_{I_k}\rfloor\mathbf{k} - {}^G_{I_{k'}}\mathbf{R}\lfloor{}^I\mathbf{p}_J\rfloor\boldsymbol{\Upsilon}_2{}^{I_{k-1}}_{I_0}\mathbf{R}\mathbf{k} - (1-\lambda){}^G_{I_0}\mathbf{R}\lfloor{}^{I_0}\mathbf{p}_{I_{k-1}}\rfloor\mathbf{k} + {}^G_{I_{k'}}\mathbf{R}\lfloor{}^I\mathbf{p}_J\rfloor{}^I_J\mathbf{R}\,{}^J_I\mathbf{R}\mathbf{k} \end{bmatrix} \tag{97}$$

$$= \begin{bmatrix} \mathbf{0}_{3\times 1} \\ -{}^G_{I_{k'}}\mathbf{R}\lfloor{}^I\mathbf{p}_J\rfloor\mathbf{k} - \lambda{}^G_{I_0}\mathbf{R}\lfloor f(t_k)\mathbf{k}\rfloor\mathbf{k} - (1-\lambda){}^G_{I_0}\mathbf{R}\lfloor f(t_{k-1})\mathbf{k}\rfloor\mathbf{k} + {}^G_{I_{k'}}\mathbf{R}\lfloor{}^I\mathbf{p}_J\rfloor\mathbf{k} \end{bmatrix} = \mathbf{0}_{6\times 1} \tag{98}$$

$$\mathbf{M}_{\mathbf{A}_k}\mathbf{N}_2 = \begin{bmatrix} \mathbf{0}_3 \\ \lambda\mathbf{I}_3 + (1-\lambda)\mathbf{I}_3 - {}^G_{I_{k'}}\mathbf{R}\,{}^I_J\mathbf{R}\,{}^J_I\mathbf{R}\,{}^{I_0}_G\mathbf{R} \end{bmatrix} = \mathbf{0}_{6\times 3} \tag{99}$$

This completes the proof. □

3.5.7 Constant Velocity 1-Axis Rotation without Translation Motion

Lemma 3.8. *If the system undergoes constant local 1-axis angular velocity motion without translation, the state is partially unobservable with directions as:*

$$\mathbf{N} = \begin{bmatrix} \mathbf{N}_1 & \mathbf{N}_2 & \mathbf{N}_3 \end{bmatrix} = \begin{bmatrix} \mathbf{k} & \mathbf{0}_{3\times1} & -{}^{I_0}\boldsymbol{\omega}_{I_0} \\ \mathbf{0}_{3\times1} & \mathbf{k} & \mathbf{0}_{3\times1} \\ \mathbf{k} & \mathbf{0}_{3\times1} & -{}^{I_0}\boldsymbol{\omega}_{I_0} \\ \mathbf{0}_{3\times1} & \mathbf{k} & \mathbf{0}_{3\times1} \\ -{}^{J}_{I}\mathbf{R}\mathbf{k} & \mathbf{0}_{3\times1} & \mathbf{0}_{3\times1} \\ \mathbf{0}_{3\times1} & {}^{J}_{I}\mathbf{R}\mathbf{k} & \mathbf{0}_{3\times1} \\ 0 & 0 & 1 \end{bmatrix} \tag{100}$$

where $\mathbf{k}$ *is the rotation axis. The relevant parameters are:* ${}^{I_k}_{G}\bar{q},\ {}^{G}\mathbf{p}_{I_k}, {}^{I_{k-1}}_{G}\bar{q},\ {}^{G}\mathbf{p}_{I_{k-1}},\ {}^{J}_{I}\bar{q},\ {}^{J}\mathbf{p}_{I},\ {}^{J}t_{I}$.

Proof. The motion constraint can be interpreted as the following geometric constraints:

$$\begin{gathered} {}^{I_0}_{G}\mathbf{R}\mathbf{k} = {}^{I_k}_{G}\mathbf{R}\mathbf{k} = \mathbf{k}, \quad {}^{I_0}\mathbf{p}_{I_k} = \mathbf{0}_{3\times1}, \quad {}^{I_k}\mathbf{v}_{I_k} = {}^{I_0}\mathbf{v}_{I_0} = \mathbf{0}_{3\times1}, \quad {}^{I_k}\boldsymbol{\omega}_{I_k} = {}^{I_0}\boldsymbol{\omega}_{I_0} = s\mathbf{k} \\ \boldsymbol{\Upsilon}_1\mathbf{k} = \lambda\mathbf{k}, \quad \boldsymbol{\Upsilon}_2\mathbf{k} = (1-\lambda)\mathbf{k}, \quad \boldsymbol{\Upsilon}_3 = \frac{{}^{I_{k-1}}_{I_k}\boldsymbol{\theta}}{t_k - t_{k-1}} = \frac{{}^{I_{k-1}}\boldsymbol{\omega}_{I_{k-1}}(t_k - t_{k-1})}{t_k - t_{k-1}} = {}^{I_{k-1}}\boldsymbol{\omega}_{I_{k-1}}, \quad \boldsymbol{\Upsilon}_4 = \mathbf{0}_{3\times1} \end{gathered} \tag{101}$$

where s is the speed of the motion.

By applying the above constraint, $\mathbf{N}$ become the null space of $\mathbf{M}_{\mathbf{A}_k}$ (only showing the new directions):

$$\begin{aligned} \mathbf{M}_{\mathbf{A}_k}\mathbf{N}_3 &= \begin{bmatrix} -{}^{J}_{I}\mathbf{R}\boldsymbol{\Upsilon}_1{}^{I_k}_{I_0}\mathbf{R}\,{}^{I_0}\boldsymbol{\omega}_{I_0} - {}^{J}_{I}\mathbf{R}\boldsymbol{\Upsilon}_2{}^{I_{k-1}}_{I_0}\mathbf{R}\,{}^{I_0}\boldsymbol{\omega}_{I_0} + {}^{J}_{I}\mathbf{R}\boldsymbol{\Upsilon}_3 \\ {}^{G}_{I_{k'}}\mathbf{R}\lfloor {}^{I}\mathbf{p}_J \rfloor \boldsymbol{\Upsilon}_1{}^{I_k}_{I_0}\mathbf{R}\,{}^{I_0}\boldsymbol{\omega}_{I_0} + \lambda{}^{G}_{I_0}\mathbf{R}\lfloor {}^{I_0}\mathbf{p}_{I_k} \rfloor {}^{I_0}\boldsymbol{\omega}_{I_0} + {}^{G}_{I_{k'}}\mathbf{R}\lfloor {}^{I}\mathbf{p}_J \rfloor \boldsymbol{\Upsilon}_2{}^{I_{k-1}}_{I_0}\mathbf{R}\,{}^{I_0}\boldsymbol{\omega}_{I_0} + (1-\lambda){}^{G}_{I_0}\mathbf{R}\lfloor {}^{I_0}\mathbf{p}_{I_{k-1}} \rfloor {}^{I_0}\boldsymbol{\omega}_{I_0} + \boldsymbol{\Upsilon}_4 - {}^{G}_{I_{k'}}\mathbf{R}\lfloor {}^{I}\mathbf{p}_J \rfloor \boldsymbol{\Upsilon}_3 \end{bmatrix} \\ &= \begin{bmatrix} -\lambda{}^{J}_{I}\mathbf{R}\,{}^{I_0}\boldsymbol{\omega}_{I_0} - (1-\lambda){}^{J}_{I}\mathbf{R}\,{}^{I_0}\boldsymbol{\omega}_{I_0} + {}^{J}_{I}\mathbf{R}\,{}^{I_{k-1}}\boldsymbol{\omega}_{I_{k-1}} \\ \lambda{}^{G}_{I_{k'}}\mathbf{R}\lfloor {}^{I}\mathbf{p}_J \rfloor {}^{I_0}\boldsymbol{\omega}_{I_0} + (1-\lambda){}^{G}_{I_{k'}}\mathbf{R}\lfloor {}^{I}\mathbf{p}_J \rfloor {}^{I_0}\boldsymbol{\omega}_{I_0} - {}^{G}_{I_{k'}}\mathbf{R}\lfloor {}^{I}\mathbf{p}_J \rfloor {}^{I_{k-1}}\boldsymbol{\omega}_{I_{k-1}} \end{bmatrix} = \mathbf{0}_{6\times1} \end{aligned} \tag{102}$$

This completes the proof. □

3.5.8 No Motion

Lemma 3.9. *If the system has no motion, the state is partially unobservable with directions as:*

$$\mathbf{N} = \begin{bmatrix} \mathbf{N}_1 & \mathbf{N}_2 & \mathbf{N}_2 \end{bmatrix} = \begin{bmatrix} \mathbf{I}_3 & \mathbf{0}_3 & \mathbf{0}_{3\times1} \\ \mathbf{0}_3 & \mathbf{I}_3 & \mathbf{0}_{3\times1} \\ \mathbf{I}_3 & \mathbf{0}_3 & \mathbf{0}_{3\times1} \\ \mathbf{0}_3 & \mathbf{I}_3 & \mathbf{0}_{3\times1} \\ -{}^{J}_{I}\mathbf{R} & \mathbf{0}_3 & \mathbf{0}_{3\times1} \\ \mathbf{0}_3 & {}^{J}_{I}\mathbf{R}{}^{I_0}_{G}\mathbf{R} & \mathbf{0}_{3\times1} \\ \mathbf{0}_{1\times3} & \mathbf{0}_{1\times3} & 1 \end{bmatrix} \tag{103}$$

The relevant parameters are: ${}^{I_k}_{G}\bar{q},\ {}^{G}\mathbf{p}_{I_k}, {}^{I_{k-1}}_{G}\bar{q},\ {}^{G}\mathbf{p}_{I_{k-1}},\ {}^{J}_{I}\bar{q},\ {}^{J}\mathbf{p}_{I},\ {}^{J}t_{I}$.

Proof. The motion constraint can be interpreted as the following geometric constraints:

$${}^{I_0}_{G}\mathbf{R} = {}^{I_k}_{G}\mathbf{R}, \boldsymbol{\Upsilon}_1 = \lambda\mathbf{I}_3, \boldsymbol{\Upsilon}_2 = (1-\lambda)\mathbf{I}_3, {}^{I_0}\mathbf{p}_{I_k} = {}^{I_k}\mathbf{v}_{I_k} = {}^{I_0}\mathbf{v}_{I_0} = {}^{I_k}\boldsymbol{\omega}_{I_k} = {}^{I_0}\boldsymbol{\omega}_{I_0} = \boldsymbol{\Upsilon}_3 = \boldsymbol{\Upsilon}_4 = \mathbf{0}_{3\times1}$$

By applying the above constraint, $\mathbf{N}$ become the null space of $\mathbf{M}_{\mathbf{A}_k}$:

$$\begin{aligned} \mathbf{M}_{\mathbf{A}_k}\mathbf{N}_1 &= \begin{bmatrix} {}^{J}_{I}\mathbf{R}\boldsymbol{\Upsilon}_1{}^{I_k}_{I_0}\mathbf{R} + {}^{J}_{I}\mathbf{R}\boldsymbol{\Upsilon}_2{}^{I_{k-1}}_{I_0}\mathbf{R} - {}^{J}_{I}\mathbf{R} \\ -{}^{G}_{I_{k'}}\mathbf{R}\lfloor {}^{I}\mathbf{p}_J \rfloor \boldsymbol{\Upsilon}_1{}^{I_k}_{I_0}\mathbf{R} - \lambda{}^{G}_{I_0}\mathbf{R}\lfloor {}^{I_0}\mathbf{p}_{I_k} \rfloor - {}^{G}_{I_{k'}}\mathbf{R}\lfloor {}^{I}\mathbf{p}_J \rfloor \boldsymbol{\Upsilon}_2{}^{I_{k-1}}_{I_0}\mathbf{R} - (1-\lambda){}^{G}_{I_0}\mathbf{R}\lfloor {}^{I_0}\mathbf{p}_{I_{k-1}} \rfloor + {}^{G}_{I_{k'}}\mathbf{R}\lfloor {}^{I}\mathbf{p}_J \rfloor {}^{I}_{J}\mathbf{R}\,{}^{J}_{I}\mathbf{R} \end{bmatrix} \\ &= \begin{bmatrix} {}^{J}_{I}\mathbf{R} - {}^{J}_{I}\mathbf{R} \\ -{}^{G}_{I_{k'}}\mathbf{R}\lfloor {}^{I}\mathbf{p}_J \rfloor + {}^{G}_{I_{k'}}\mathbf{R}\lfloor {}^{I}\mathbf{p}_J \rfloor \end{bmatrix} = \mathbf{0}_{6\times3} \end{aligned} \tag{104}$$

$$\mathbf{M}_{\mathbf{A}_k}\mathbf{N}_2 = \begin{bmatrix} \mathbf{0}_3 \\ \lambda\mathbf{I}_3 + (1-\lambda)\mathbf{I}_3 - {}^{G}_{I_{k'}}\mathbf{R}{}^{I}_{J}\mathbf{R}{}^{J}_{I}\mathbf{R}{}^{I_0}_{G}\mathbf{R} \end{bmatrix} = \mathbf{0}_{6\times3}, \qquad \mathbf{M}_{\mathbf{A}_k}\mathbf{N}_3 = \begin{bmatrix} {}^{J}_{I}\mathbf{R}\boldsymbol{\Upsilon}_3 \\ \boldsymbol{\Upsilon}_4 - {}^{G}_{I_{k'}}\mathbf{R}\lfloor {}^{I}\mathbf{p}_J \rfloor \boldsymbol{\Upsilon}_3 \end{bmatrix} = \mathbf{0}_{6\times1} \tag{105}$$

This completes the proof. □

4 More Numerical Studies

In this section, we show two numerical studies: the effect of different IMU noise levels on the inconsistency of state estimation and verifying the generalizability of our analysis to general multi-sensor fusion-based navigation systems.

4.1 Ablation Study: Different IMU Noise Levels

We tested with 3 different levels of IMU noise changing the white noise level of gyroscope and accelerometer measurements (biases remain the same). Specifically, we set the noise levels as: 1.0e-5, 1.0e-3, and 1.0e-1, and the results are shown in Fig. 13, 14, and 15. We used a 1-axis rotation with constant velocity motion trajectory for these tests.

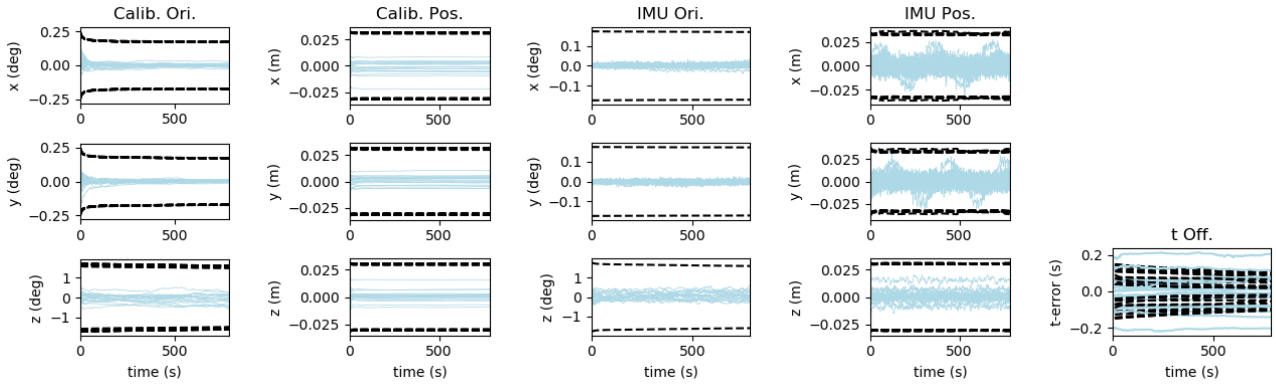

Figure 13: State estimation with online calibration performance with IMU noise 1.0e-5.

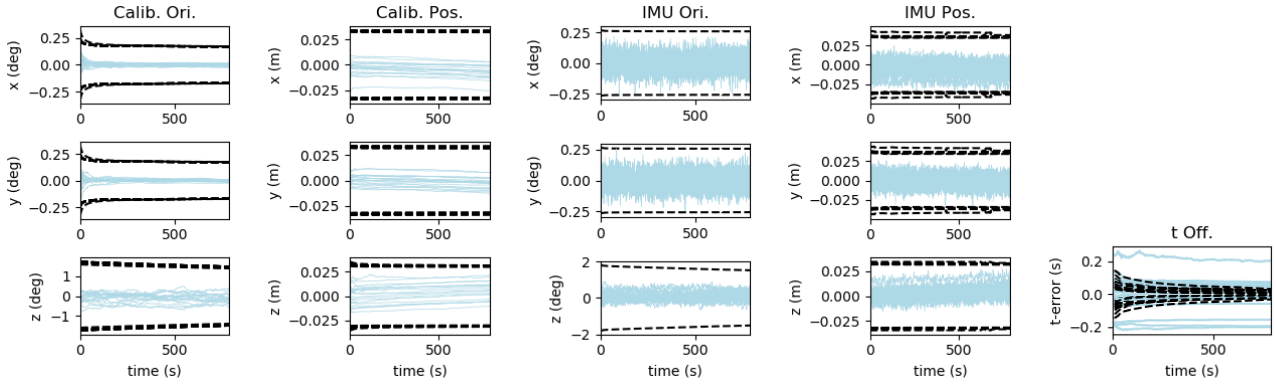

Figure 14: State estimation with online calibration performance with IMU noise 1.0e-3.

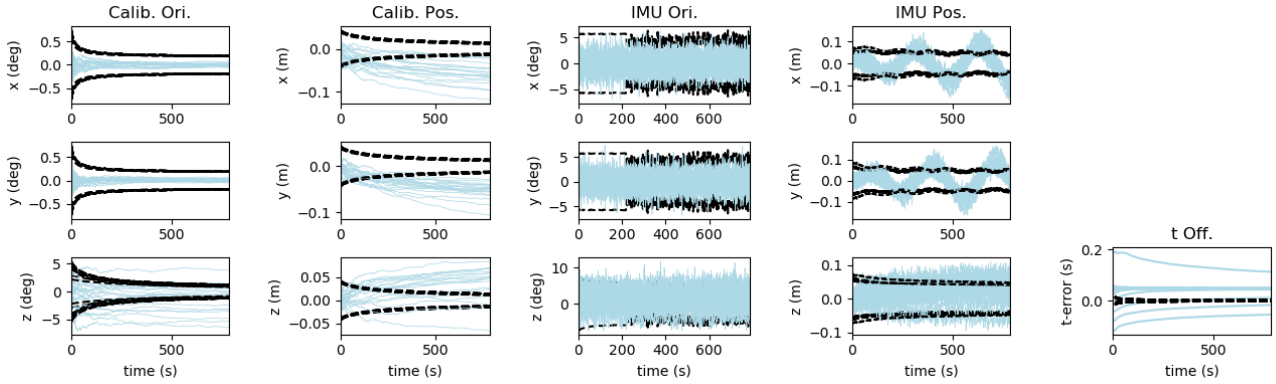

Figure 15: State estimation with online calibration performance with IMU noise 1.0e-1.

It is clear that with lower-noise IMU, the overall estimation performances are more consistent while with higher-noise IMU, the estimation becomes more inconsistent under *the same degenerate motion*.

This can be considered as the lower-noise IMU provides more information and allows higher accuracy of state estimation reducing the gain of wrong information toward the unobservable directions of the state by lowering input of the errors, such as linearization errors, randomness from the noise, and numerical errors.

4.2 Generalization to Multi-Sensor Systems

In this section, we further extend our analysis to general multi-sensor systems, including Camera-IMU, GPS-IMU, LidAR-IMU, and Camera-GPS-LiDAR-IMU. Here we show a 1-axis translation motion trajectory case (see Fig. 2c and 3) and the results are shown in Fig. 16, 17, 18, and 19.

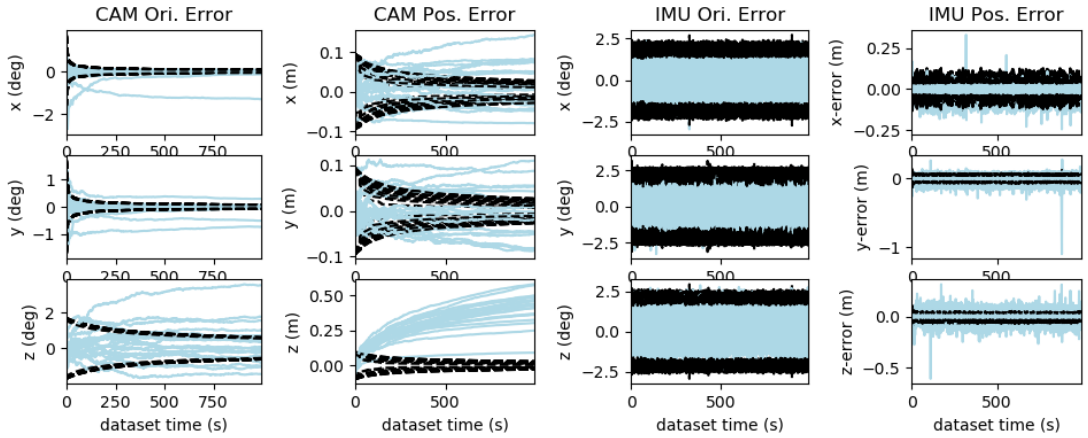

Figure 16: Camera-IMU: State estimation with online calibration performance across 20 Monte-Carlo simulations where the blue lines are the estimation error and black lines indicate the $\pm 3\sigma$ bounds

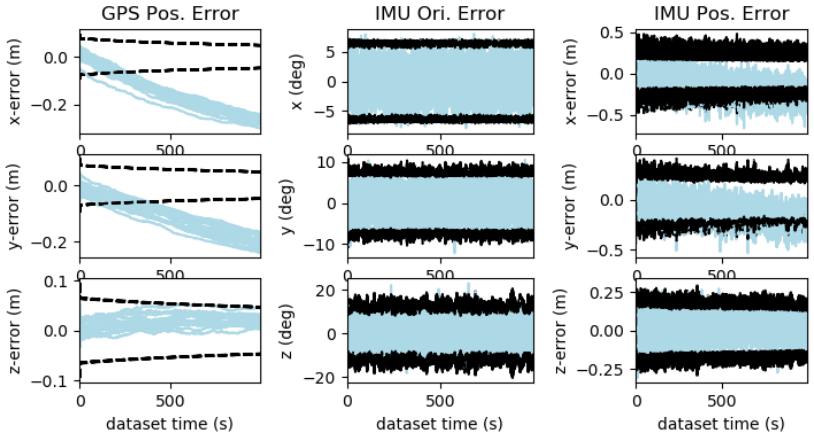

Figure 17: GPS-IMU: State estimation with online calibration performance across 20 Monte-Carlo simulations where the blue lines are the estimation error and black lines indicate the $\pm 3\sigma$ bounds

The results show that these systems have similar inconsistency under the degenerate motions; the most apparent tendency is the estimation drift of both sensor calibration position and IMU position (*Lemma 2.5* and *Lemma 3.5*) regardless of sensor combinations which indicates that these systems under the degenerate motion have the same unobservable directions of the state.

As noted earlier, the camera and LiDAR are in general not considered as global sensors. However, the global pose information can be inferred from their measurements (refer to Appendix A and C of [1]) which place the systems using these sensors under the influence of the same degenerate motions. This allows our analysis to be applied to general multi-sensor fusion-based navigation systems (with spatiotemporal calibration) which help understand the observability of most systems under the identified degenerate motions.

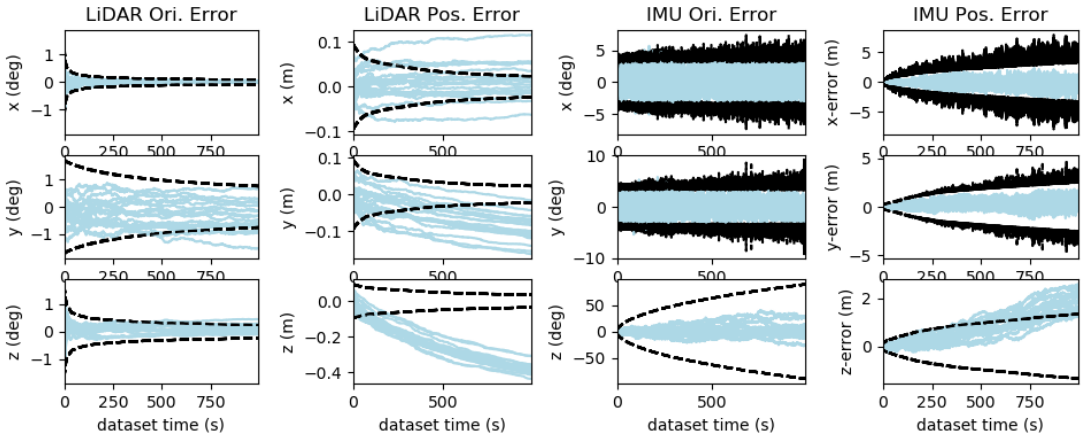

Figure 18: LidAR-IMU: State estimation with online calibration performance across 20 Monte-Carlo simulations where the blue lines are the estimation error and black lines indicate the $\pm 3\sigma$ bounds

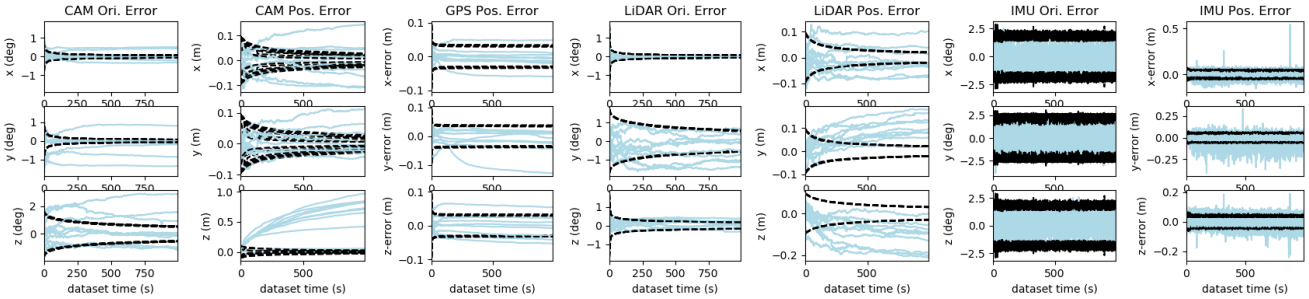

Figure 19: Camera-GPS-LiDAR-IMU: State estimation with online calibration performance across 20 Monte-Carlo simulations where the blue lines are the estimation error and black lines indicate the $\pm 3\sigma$ bounds

References

[1] Woosik Lee, Patrick Geneva, Chuchu Chen, and Guoquan Huang. "MINS: Efficient and Robust Multisensor-aided Inertial Navigation System". In: *arXiv preprint arXiv:2309.15390* (2023). URL: https://github.com/rpng/MINS.

[2] Nikolas Trawny and Stergios I. Roumeliotis. *Indirect Kalman Filter for 3D Attitude Estimation*. Tech. rep. University of Minnesota, Dept. of Comp. Sci. & Eng., Mar. 2005.

[3] Christoph Hertzberg, René Wagner, Udo Frese, and Lutz SchröDer. "Integrating Generic Sensor Fusion Algorithms with Sound State Representations Through Encapsulation of Manifolds". In: *Information Fusion* 14.1 (Jan. 2013), pp. 57–77. ISSN: 1566-2535.

[4] Gregory Chirikjian. *Stochastic Models, Information Theory, and Lie Groups, Volume 2: Analytic Methods and Modern Applications*. Vol. 2. Springer Science & Business Media, 2011.

[5] Zhe Chen, Ke Jiang, and James C Hung. "Local observability matrix and its application to observability analyses". In: *[Proceedings] IECON'90: 16th Annual Conference of IEEE Industrial Electronics Society*. IEEE. 1990, pp. 100–103.

[6] Mingyang Li. "Visual-Inertial Odometry on Resource-Constrained Systems". PhD thesis. UC Riverside, 2014.

[7] Yulin Yang, Patrick Geneva, Kevin Eckenhoff, and Guoquan Huang. "Degenerate Motion Analysis for Aided INS with Online Spatial and Temporal Calibration". In: *IEEE Robotics and Automation Letters (RA-L)* 4.2 (2019), pp. 2070–2077.

[8] Faraz M Mirzaei and Stergios I Roumeliotis. "A Kalman filter-based algorithm for IMU-camera calibration: Observability analysis and performance evaluation". In: *IEEE transactions on robotics* 24.5 (2008), pp. 1143–1156.